AGU ADVANCING EARTH AND SPACE SCIENCE

Water Resources Research

RESEARCH ARTICLE
10.1029/2021WR030332

Key Points:

- We apply hydraulic mixing-cell modeling at an intensively-studied test site and highlight its complementary asset to field investigations
- Contrary to expectation, we found small spatial variance of how and from where surface water is sourced to the riparian-stream continuum
- Sources were also similar for wetting and drying but we found a gradual activation of different subsurface stores with increasing wetness

Correspondence to:
J. Klaus,
julian.klaus@uni-bonn.de

Citation:
Glaser, B., Hopp, L., Partington, D., Brunner, P., Therrien, R., & Klaus, J., (2021). Sources of surface water in space and time: Identification of delivery processes and geographical sources with hydraulic mixing-cell modeling. *Water Resources Research*, *57*, e2021WR030332. https://doi.org/10.1029/2021WR030332

Received 1 MAY 2021
Accepted 6 OCT 2021

Author Contributions:
Conceptualization: Barbara Glaser, Luisa Hopp, Philip Brunner, Julian Klaus
Data curation: Barbara Glaser
Formal analysis: Barbara Glaser
Funding acquisition: Barbara Glaser, Julian Klaus
Investigation: Barbara Glaser
Methodology: Barbara Glaser, Luisa Hopp, Daniel Partington, Julian Klaus
Project Administration: Barbara Glaser, Julian Klaus
Software: Barbara Glaser, Daniel Partington, Philip Brunner, René Therrien
Supervision: Luisa Hopp, Julian Klaus
Validation: Barbara Glaser, Luisa Hopp, Julian Klaus
Visualization: Barbara Glaser
Writing – original draft: Barbara Glaser

Sources of Surface Water in Space and Time: Identification of Delivery Processes and Geographical Sources With Hydraulic Mixing-Cell Modeling

Barbara Glaser[1,2,3], Luisa Hopp[2], Daniel Partington[4], Philip Brunner[5], René Therrien[6], and Julian Klaus[1,7]

[1]Catchment and Eco-Hydrology Research Group, Luxembourg Institute of Science and Technology, Esch/Alzette, Luxembourg, [2]Department of Hydrology, University of Bayreuth, Bayreuth, Germany, [3]Now at Bavarian Environment Agency, Augsburg, Germany, [4]National Centre for Groundwater Research and Training, and College of Science and Engineering, Flinders University, Adelaide, SA, Australia, [5]Centre for Hydrogeology and Geothermics, University of Neuchâtel, Neuchâtel, Switzerland, [6]Department of Geology and Geological Engineering, Laval University, Laval, QC, Canada, [7]Now at Institute of Geography, University of Bonn, Bonn, Germany

Abstract Knowledge of the sources of surface water in riparian zones and floodplains is critical to understanding its role in runoff generation and impact on biogeochemical and ecological processes. In this study, we demonstrate the potential of integrated surface-subsurface hydrologic modeling (HydroGeoSphere) in combination with a hydraulic mixing-cell approach to decipher different sources of surface water and their mixing in space and time. We present a novel approach to processing the model data that allowed us to compare which mechanisms ultimately transferred water to the surface (delivery processes) and from where the surface water originated (geographical sources) for varying wetness states and phases of wetting or drying across 36 test locations within the riparian-stream continuum of an intensively-studied, humid-temperate, forested headwater catchment (45 ha). Consistent with current process understanding for the study site, water exfiltrating from the subsurface was simulated as the dominant source for riparian surface water and intermittent streamflow. The model further helped to specify the relevance of different subsurface stores, revealing a wetness-dependent activation of upslope source areas. Contributions of riparian overland flow and precipitation were minor during all investigated phases of wetting and drying. Moreover, the spatial variability of surface water sources proved to be smaller than expected for the heterogeneous patterns and frequencies of the surface saturation observed and simulated. Based on these findings, we discuss the value of hydraulic mixing-cell modeling to complement the planning and interpretation of field investigations and to enhance process understanding regarding the spatio-temporal sources of surface water.

1. Introduction

Floodplains and riparian zones are critical landscape units for a wide range of hydrological, biogeochemical, and ecological processes. A main characteristic of these ecohydrological interfaces (cf. Krause et al., 2017) is irregular inundation in space and time. The spatial and temporal variability of water availability creates specific microhabitats for flora and fauna (e.g., Mallik et al., 2001; Ramey & Richardson, 2017) and hot spots and hot moments of biogeochemical activity (e.g., Frei et al., 2012; Harms & Grimm, 2008; Singer et al., 2016), which in turn can influence water quantity and quality (e.g., Grabs et al., 2012; Williams & Scott, 2009). Moreover, for flood risk assessment, it is important to understand where and when water accumulates at the surface of floodplains and riparian zones and how it potentially contributes to streamflow generation via overland flow.

Several processes can induce standing and flowing water at the landscape surface (cf. e.g., Dunne & Black, 1970; Hewlett & Hibbert, 1967; Megahan & King, 1985). Surface water can originate from the exfiltration of subsurface water and from precipitation ponding due to infiltration or saturation excess. The continued delivery of water from the subsurface or from precipitation expands surface saturation via overland flow. In addition, an expansion of streamflow can induce surface saturation in riparian zones or floodplains, even though streamflow is essentially generated either by the exfiltration of subsurface water or the infiltration excess or saturation excess of precipitation. Depending on the mechanism responsible for

Writing – review & editing: Barbara Glaser, Luisa Hopp, Daniel Partington, Philip Brunner, René Therrien, Julian Klaus

the generation of surface saturation, the origin and characteristics of surface water can vary, leading to potentially different impacts on ecology, water quality, runoff, and flood risk. It is therefore necessary to understand the processes that dominate the generation of surface saturation, identify the sources of water contributing to surface water, and quantify the spatial and temporal variabilities of different sources of surface water and their mixing. Yet, although one of the most prominent challenges in catchment hydrology is to identify where stream water comes from (e.g., Hewlett & Hibbert, 1967; McDonnell, 2003), few efforts have been made to date to investigate and differentiate between the sources of surface water in floodplains and in the riparian-stream continuum.

An investigation into the sources of surface water may focus on three different aspects (cf. Sklash & Farvolden, 1979): (a) How old is the water, that is, what are the temporal sources? (b) Where does the water come from, that is, what are the geographical sources? (c) Which mechanisms ultimately transferred the water to the surface, that is, what are the delivery processes? A large number of studies have investigated one or two of these three aspects for stream hydrographs based on physical measurements of water fluxes, hydrological tracers, and mixing analyses (cf. literature overviews given in Barthold & Woods, 2015; Cowie et al., 2017; Klaus & McDonnell, 2013). Numerous experimental studies demonstrated that the mixing of water from different subsurface stores and landscape units, the ratio of event and pre-event water, and the distribution of water age in the hydrograph change within and between runoff events and for different seasons and wetness conditions (e.g., Birkel et al., 2012; Cartwright & Morgenstern, 2018; Correa et al., 2017; Martinez-Carreras et al., 2015; McGlynn & Seibert, 2003). Others analyzed how the mixture of streamflow sources changes spatially depending on the catchment size or other landscape characteristics (e.g., Correa et al., 2019; Cowie et al., 2017; Gordon et al., 2015; Kirchner, 2009; Laudon et al., 2007; McGlynn et al., 2004; Zhang et al., 2018). However, we are aware of only very few studies that collected field data to investigate the spatial variability of surface water sources over short distances along the stream channel (Brown et al., 1999) or for inundated areas in the riparian zone or floodplains (Berezowski et al., 2019; Beumer et al., 2007; Bonnet et al., 2017).

Comprehensive spatial and temporal sampling of water sources is limited by high labor and cost requirements (e.g., Correa et al., 2019). The sampling of surface water in the riparian zone or floodplains is further complicated by the intermittent occurrence and commonly low depth of water. Thus, hydrologic modeling can be a useful complement to field studies to track and analyze the sources of surface water. Various recent studies have developed and applied models with particle tracking schemes to simulate transient travel and residence time distributions, that is, the dynamics of the temporal sources of surface water (e.g., de Rooij et al., 2013; Engdahl & Maxwell, 2015; Maxwell et al., 2019; Remondi et al., 2018; Wilusz et al., 2020; Yang et al., 2018). Others have applied solute transport simulations and particle tracking to identify temporal or geographical sources of streamflow (e.g., Chow et al., 2016; Jones et al., 2006; Liggett et al., 2014). Moreover, methods were developed to estimate and track the mixing of different geographical and temporal water sources on a cell-by-cell basis throughout the simulation domain (Partington et al., 2011, 2013; Sayama & McDonnell, 2009). All these different approaches are valuable options to extract detailed information on water sources from simulations as a complement to field observations. With regards to the spatio-temporal variability of sources of surface water, the approaches are most valuable when applied in integrated surface-subsurface hydrologic models (ISSHMs). This is because ISSHMs do not require *a priori* definitions of the extent of surface water bodies and the exchange of water between the surface and subsurface, but explicitly simulate the dynamic development of surface water according to the internal model state (cf. e.g., Berg & Sudicky, 2019; Kollet et al., 2017; Maxwell et al., 2014; Paniconi & Putti, 2015; Sebben et al., 2013).

Despite the range of available approaches to simulate, track, and analyze sources of surface water in space and time, to date, only a few studies have made use of ISSHMs to investigate surface water sources across space. Weill et al. (2013) analyzed simulated exchange fluxes between the surface and subsurface to decipher the mechanisms generating surface saturation across the hillslopes and the riparian zone of a small pre-alpine headwater catchment. Similarly, Partington et al. (2013) investigated the generation of overland flow and stream flow in a riparian wetland during a storm event, applying and further developing a hydraulic mixing-cell approach (Partington et al., 2011) that estimates the mixing of water originating from different source areas based on the hydraulic fluxes and fluid volumes simulated with ISSHMs. Gutiérrez-Jurado et al. (2019) applied this mixing-cell approach (Partington et al., 2011, 2013) in numerical experiments to

identify how and where intermittent streams are initiated and sourced, depending on different characteristics representative for low-gradient catchments with a Mediterranean climate. The three above-mentioned studies demonstrated that the dominating processes for the generation of surface saturation varied locally due to spatio-temporally varying conditions, such as soil type and antecedent wetness. However, the main aim of all three studies was to identify the contribution of overland flow to streamflow generation rather than to analyze the sources of surface saturation outside the stream channel, and performance of the simulations was, if at all, only verified against discharge at the catchment outlet. The only study we are aware of that used ISSHM simulations to explicitly analyze the sources of surface water outside the stream channel, including a detailed verification of the spatial model output, is a recent study by Berezowski et al. (2019). The authors successfully applied the hydraulic mixing-cell approach developed by Partington et al. (2011, 2013) to analyze the complexity of the geographical sources of surface water within the 250 km^2 floodplain of the Biebrza River catchment, in Poland, focusing on the spatial extent and dynamic movement of the active perirheic zone, that is, the area where water from the stream channel and from the floodplain mix.

In this study, we apply the ISSHM HydroGeoSphere (Aquanty Inc., 2018; Brunner & Simmons, 2012) combined with the hydraulic mixing-cell approach (Partington et al., 2011, 2013) to decipher the spatio-temporal variability of delivery processes and geographical sources of surface water in the riparian-stream continuum of a small intermittent stream. Our test site is the intensively studied 42 ha Weierbach catchment (Luxembourg), where previous work has shown that HydroGeoSphere can accurately simulate the dynamics, patterns, and frequencies of the surface saturation occurrence (Glaser et al., 2020) observed for several distinct riparian-stream areas with repeated thermal infrared imagery mapping (Antonelli et al., 2020a; Glaser et al., 2018). The thermal infrared imagery suggested that there were distinct locations where subsurface water exfiltration induced and maintained surface saturation in the riparian zone, while additional surface water may have originated either from the stream extending into the riparian zone or from precipitation. In line with these observations, the HydroGeoSphere simulation (Glaser et al., 2020) implied that surface saturation in the Weierbach catchment mainly originated from groundwater exfiltration into microtopographic depressions (extent of tens of centimeters to a few meters). However, the contribution of additional water sources to the spatio-temporal occurrence of surface water remained unknown from the standard model output.

The overall objective of our study is to explore to what extent ISSHM hydraulic mixing-cell simulations can provide insight into the spatial and temporal variability of sources of surface water in the riparian-stream continuum and can thus complement and enhance the possibilities of field studies and standard simulations for improved process understanding. In particular, we apply the hydraulic mixing-cell simulations across the riparian zone and stream channel of an upstream, a midstream, and a downstream location in the experimental Weierbach catchment for periods with different initial wetness conditions and phases of wetting and drying, and seek to identify:

1. Which mechanisms ultimately induce and maintain the occurrence of water at the surface, that is, what are the delivery processes, in space and time?
2. From which landscape units and subsurface stores does the surface water originate, that is, what are the geographical sources of surface water, in space and time?

2. Study Site and Previous Work

2.1. Weierbach Catchment

The Weierbach catchment is a forested catchment (42 ha) in western Luxembourg. The stream network consists of three tributaries that merge into a main stream flowing through a steep, v-shaped stream valley (Figure 1). The stream is bordered by a narrow, flat riparian zone that widens at several sections along the stream and around the heads of the three tributaries (Figure 1). The riparian zone comprises 1.2% of the catchment area and is vegetated with ferns, mosses, and herbaceous plants. Hillslopes (slopes >5°, 45% of catchment area) and the plateau (slopes <5°, 54% of catchment area) are covered by deciduous forest (mainly European beech, Sessile oak) with some patches of coniferous trees, and by a coniferous forest (mainly Norway spruce and Douglas spruce) in the south-east of the catchment.

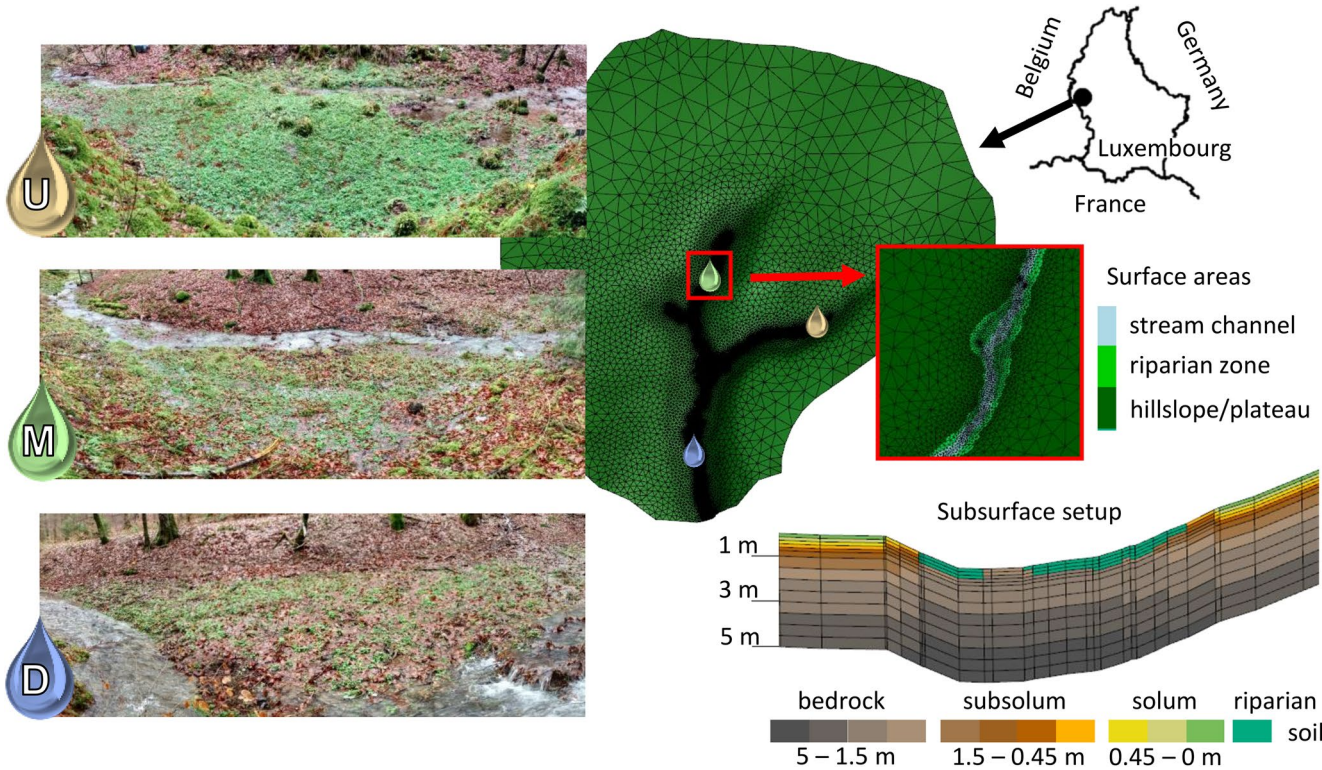

Figure 1. Model setup of the 42 ha Weierbach catchment in western Luxembourg. The three riparian-stream areas investigated in this study are located at an upstream section at the eastern tributary (*U*, 155 m^2), a midstream section at the middle tributary (*M*, 169 m^2), and a downstream section at the main stream (*D*, 170 m^2). The nested model mesh is colored according to the delineation of the surface domain into hillslopes and plateau, riparian zone, and stream channel. The profile at the bottom right shows the vertical discretization of the subsurface model domain and the assigned parameterization zones in and adjacent to the riparian zone, corresponding to the fresh and fractured bedrock (slate and phyllites), the subsolum (regolithic saprock), the solum of the hillslopes and plateau (Cambisol), and the riparian soil (Leptosol) of the catchment.

The catchment bedrock is dominated by fractured Devonian slates and phyllites. The fracture density gradually decreases from the top of the bedrock at a depth of about 1.4 m to essentially non-fractured fresh bedrock in about 5 m (Gourdol et al., 2021). A subsolum classified as regolithic saprock (cf. Juilleret et al., 2016) and a shallow Cambisol (average solum depth 0.5 m) overlie the fractured bedrock on the plateau and hillslopes of the catchment. In the riparian zone, the bedrock is overlain by a shallow organic Leptosol (cf. Glaser et al., 2016), while it outcrops in the stream channel (cf. Figure 1).

The climate is oceanic-continental with an average annual precipitation of around 950 mm and average annual potential evapotranspiration of around 590 mm (cf. Carrer et al., 2019; Pfister et al., 2017; data based on years 2006–2014). Precipitation is distributed rather uniformly over the year, while evapotranspiration and runoff (annual average around 480 mm) show clear seasonal variations (cf. Pfister et al., 2017). During dry conditions, streamflow intermittently ceases from upstream to downstream and rainfall-runoff behavior is characterized by sharp, short-lasting discharge peaks. During wet conditions, additional response shows in the form of a broad, long-lasting second discharge peak that starts to appear few hours after the onset of precipitation and largely outweighs the volume of the first discharge peaks (e.g., Martinez-Carreras et al., 2016; Scaini et al., 2018).

2.2. Weierbach Model

In this study, we use the integrated surface-subsurface hydrologic model HydroGeoSphere (HGS, Aquanty Inc., 2018) as previously implemented for the Weierbach catchment (Glaser et al., 2020). The model consists of a 5-m deep subsurface domain where transient subsurface flow is simulated with the 3D Richards equation and a surface domain in which surface flow is simulated with the diffusive-wave approximation

of the 2D Saint-Venant equation. Surface and subsurface flow are simulated simultaneously and the exchange between the two domains is simulated with the dual node approach, that is, as Darcy flow through a thin coupling layer (10^{-4} m). Actual evapotranspiration is simulated based on potential evapotranspiration, actual water availability, and some plant and soil characteristics (e.g., rooting depth, evaporation depth) following the conceptual approach of Kristensen and Jensen (1975).

The surface domain is spatially discretized into 42,274 triangular elements with edge lengths ranging from >30 m on the plateau to <0.4 m in the riparian zone and stream channel (Figure 1). The triangular mesh was generated with AlgoMesh (HydroAlgorithmics Pty Ltd, 2016) and elevation of the surface nodes was interpolated from a 0.1 m elevation raster (cf. Glaser et al., 2016). The triangular mesh was extruded in the third dimension to discretize the subsurface domain with fourteen layers of triangular prisms with vertical thicknesses ranging from 0.15 m for the top layers to 0.5 m for the bottom layers (cf. Figure 1). The sides and the bottom of the subsurface domain are no-flow boundaries. A critical depth boundary is assigned along the sides of the surface domain to allow water to leave the model domain.

The parameterization of the model subsurface distinguishes twelve different property layers representing the specific pedolithology of the catchment with solum, subsolum, fractured bedrock, and a different soil type in the riparian zone (cf. 2.1, Figure 1). The subsurface is set up homogeneously across the hillslopes and plateau, whereas the upper property layers are removed in the riparian zone and stream channel and replaced by riparian soil and lower property layers in dependency of the topography (cf. Figure 1 and Glaser et al. (2016) for details on the implementation). Evapotranspiration parameters and Manning's surface roughness differ between the deciduous and coniferous forest, the riparian zone, and the stream channel. All surface and subsurface parameter values are given and detailed in Glaser et al. (2020). Here, it should be noted that the model parameters were not calibrated at catchment scale, but were transferred from an HGS model implementation of a 6 ha headwater area of the middle tributary (Glaser et al., 2016). The parameterization of this 6 ha headwater catchment was largely based on field experience and measurements (e.g., ERT profiles, soil profiles, hydraulic conductivity measurements) and literature values. Only some evapotranspiration parameters, porosity values, and hydraulic conductivity were adapted in a manual calibration procedure at headwater scale (cf. Glaser et al., 2016).

Glaser et al. (2020) simulated the hydraulic states and fluxes in the Weierbach catchment from October 2015 to January 2018, driving them with daily input data of precipitation recorded within the catchment and potential evapotranspiration (FAO reference evapotranspiration) calculated from meteorological data from nearby weather stations. A multi-data evaluation showed that simulated discharge, groundwater level, and soil moisture matched observation data well. Kling Gupta efficiency was 0.74 for the simulated discharge at the catchment outlet and ranged from 0.47 to 0.49 for the simulated discharge of the three tributaries. The seasonal dynamic of groundwater levels was captured at all five monitoring locations distributed across the catchment (Pearson correlation coefficients r ranging between $r = 0.62$ and $r = 0.84$) and groundwater level was captured particularly well for locations in and close to the riparian zone. Simulated water content showed some deficiencies during dry conditions, but captured the overall seasonal soil moisture dynamics at different locations and in different depths ($r = 0.73 \pm 0.15$).

2.3. Surface Saturation in the Riparian-Stream Continuum of the Weierbach Catchment

Several experimental and modeling studies have suggested that riparian water and riparian overland flow are important contributors to event runoff generation in the Weierbach catchment (Fenicia et al., 2014; Glaser et al., 2016; Klaus et al., 2015; Martinez-Carreras et al., 2015, 2016; Rodriguez & Klaus, 2019; Schwab et al., 2018; Wrede et al., 2015). Furthermore, a recent characterization of the seasonal dynamics of surface saturation in seven distinct riparian-stream areas of the catchment revealed a largely synchronous development of surface saturation across space, but some spatial variability in both the relationships between the local extent of surface saturation and the catchment discharge and the local extent of surface saturation and the discharge of the associated stream reach (Antonelli et al., 2020a, 2020b). The extent and dynamics of the surface saturation analyzed in Antonelli et al. (2020a, 2020b) for the period October 2015 to January 2018 were derived from a comprehensive data set of weekly to biweekly thermal infrared images. This employment of thermal infrared imagery implies that surface saturation was defined as water standing or flowing at the surface, excluding “mere” saturation in the top soil layer, where water does not appear on the

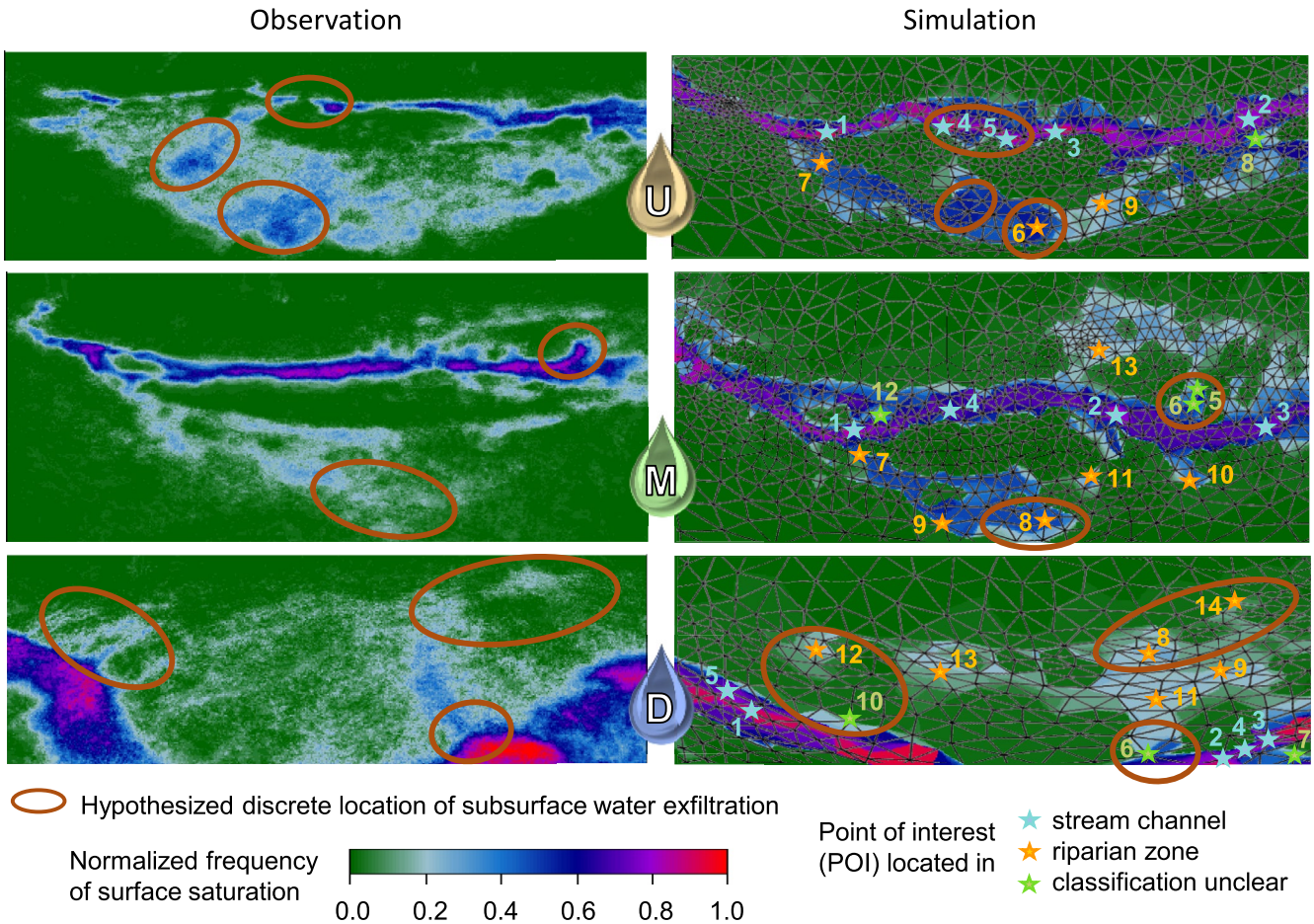

Figure 2. Patterns of observed (left) and simulated (right) frequency of surface saturation in the three investigated riparian-stream areas (cf. Figure 1). The observed frequencies indicate how often surface water was standing or flowing within the riparian zone and stream channel over the entity of 43 (*U*), 48 (*M*), and 37 (*D*) thermal infrared image snapshots taken between October 2015 and January 2018 (cf. Figure 4, Glaser et al., 2020). The simulated frequencies indicate how often water was simulated in the surface domain (water depth $>10^{-4}$ m) during the same moments in time (cf. Glaser et al., 2020). Locations that were presumed locations of discrete subsurface water exfiltration based on the field observations are labeled with brown circles. Points of interest (POIs) that were selected for detailed analyses with the hydraulic mixing-cell simulations (cf. Section 3) are colored depending on their location in the riparian zone (yellow stars) or stream channel (blue stars) and numbered according to decreasing saturation frequency within the different areas. Figure adapted from Glaser et al. (2020).

soil surface, but including stream water (cf. Glaser et al., 2018; Pfister et al., 2010). Glaser et al. (2020) used the same comprehensive data set of thermal infrared images and the same definition of surface saturation to validate the HGS model of the Weierbach catchment (cf. Section 2.2) and showed that the model could satisfactorily reproduce the observed dynamic patterns of surface saturation for the different investigated riparian-stream areas, including the spatial patterns of surface saturation frequency (Figure 2).

Glaser et al. (2020) concluded from the simulations that the generation of surface saturation in the Weierbach catchment is largely driven by groundwater exfiltration into topographic depressions, which matches evidence from the thermal infrared field observations (Antonelli et al., 2020a, 2020b; Glaser et al., 2018). However, field observations and simulations suggested that exfiltration from the subsurface is not the only source for water at the surface. The thermal infrared imagery indicated that the delivery of subsurface water to the surface is maintained at discrete exfiltration locations (Figure 2). These discrete locations of subsurface water exfiltration were derived based on the temperatures monitored with the recurrent thermal infrared imagery, the identified surface saturation frequencies, and the observed stability of the surface saturation over time. Surface saturation at other locations was not related exclusively to the exfiltration of subsurface water, but to additional delivery processes, that is, overland flow from the discrete exfiltration

locations through the riparian zone, streamflow from upstream potentially extending into the riparian zone, and precipitation. Glaser et al. (2020) further suggested that the spatial patterns of surface saturation frequency observed and simulated within the investigated areas are related to spatially varying mixtures of water sources and delivery processes, such as an obviously more dominant delivery of water from upstream via streamflow in the stream channel than in the less frequently saturated riparian zone (cf. Figure 2).

3. Application of Hydraulic Mixing-Cells to Identify Surface Water Sources

3.1. Hydraulic Mixing-Cell Approach

The hydraulic mixing-cell (HMC) approach is a modified mixing-cell approach developed for integrated surface-subsurface hydrologic models by Partington et al. (2011, 2013). It enables tracking and delineation of the mixing of predefined initial water sources at any location and at any time based on information from the hydraulic flow solution. The method is, in principle, applicable to any spatially-distributed surface-subsurface hydrological model, regardless of whether the model relies on a cell-centered or node-centered, finite volume, finite element, or finite difference scheme (Partington et al., 2011). For node-centered models such as HGS, mixing cells are conceptualized around the mesh nodes, comprising proportionate parts of the adjacent model elements according to the finite element basis function (Partington et al., 2011). Each mixing cell of the surface and subsurface domain is assigned to a source area, and water that was initially stored within the cell is tracked as water from the respective source area throughout the simulation. Water newly entering the model system during the simulation via precipitation is assigned as precipitation throughout the simulation. Thus, the water keeps the initial source assignment when passing through cells of different source areas, and the output of the HMC approach shows if and where water was stored at the start of the simulations. However, water originating from different source areas mixes within the cells and the mixing ratio is tracked and updated throughout the simulation. This conceptualization implies that in the early phase of a simulation, the mixing cells are filled by a mixture of water that initially (i.e., at the start of the simulation) was stored in sources areas in the proximity of the mixing cell and is mobilized on fast flow paths. With progressing simulation time, this water is gradually flushed out and replaced by water that needs more time to reach the mixing cell (i.e., water initially originating from more distant source areas or moving along slow flow paths) and by water newly entering the system via precipitation (which eventually will remain the only source after long simulation periods). This general change of the mixture of water sources in the mixing cells with progressing time of a HMC simulation has to be considered for the choice of an appropriate time span of the HMC simulation and in the analysis of the tracked mixing ratios according to the research aim.

The mixing ratio comprises the entirety of the individual relative contributions of the different sources to the total water volume. The fractions (i.e., relative contributions) of different water sources in a mixing cell are calculated based on the simulated hydraulic fluxes into and out of the mixing cell, the fluid volume in the cell, and the assumption that water mixes within the cell following the "modified mixing rule", that is, mixing follows a regime that ranges between perfect mixing and piston flow (cf. Campana & Simpson, 1984). In order to avoid numerical instability and numerical dispersion while ensuring computational efficiency, the possibility of calculating mixing ratios for sub-time-steps of the flow solution and several stability criteria were introduced (cf. Partington et al., 2013). These stability criteria are checked at each time step and for each mixing cell individually, and if one criterion is not met, the affected cell is excluded from the mixing calculation of the current time step. Instead, the fractions of water sources in the cell are reset and the cell is assigned a so-called reset fraction of 1. This reset fraction is also tracked in the course of the simulation and indicates an unknown origin of water.

3.2. HMC Simulation in the Weierbach Catchment

We analyzed the sources of surface water with the HMC approach for 36 distinct points of interest (POIs) in the riparian zone and stream channel of the Weierbach catchment. The POIs were distributed within three riparian-stream areas, comprising an upstream (*U*, 155 m^2), a midstream (*M*, 169 m^2), and a downstream (D, 170 m^2) section of the stream (cf. Figure 2). As POIs, we selected mesh nodes of the surface domain of the HGS model (cf. Section 2.2) that covered a large range of different saturation frequencies (cf. order number

of the POIs, Figure 2) as well as nodes that were located in the stream channel (blue labeled POIs, Figure 2), in the riparian zone (yellow labeled POIs, Figure 2), at locations that could not unambiguously be assigned to the stream channel or riparian zone (green labeled POIs, Figure 2), and at locations with a presumed distinct exfiltration of subsurface water (POIs within brown circles, Figure 2).

To identify different sources of surface water with the HMC approach, we distinguished between incoming precipitation and seven different source areas. The source areas corresponded to the zones of the model parameterization (cf. Section 2.2), with three source areas for the surface domain, namely hillslopes and plateau, riparian zone, and stream channel, and four source areas for the subsurface domain, namely fractured bedrock, subsolum, solum of the hillslopes and plateau, and riparian soil (cf. Figures 1 and 3). These predefined source areas allowed us to differentiate between several delivery processes and geographical sources of surface water with the HMC simulation (see Section 3.3). In addition, the HMC simulation provides basic information on the temporal sources of surface water, since one can separate "new" water that entered the system during the simulation as precipitation from "old" water that was already stored at the surface or in the subsurface at the start of the simulation (cf. Section 3.1).

We ran the HMC-enabled HGS model from October 2015 to January 2018 with hourly meteorological forcing data. The simulation period corresponds to the period for which Glaser et al. (2020) proved confidence in the model realism by a comprehensive validation of the HGS model against hydrometric measurements (cf. Section 2.2.) and patterns and frequencies of surface saturation mapped within the riparian-stream areas (cf. Section 2.3, Figure 2). In order to deal with the effect that the signal of initially stored water is successively flushed out and eventually fully replaced by new incoming precipitation in a HMC simulation (cf. Section 3.1), we split the 28-month HMC simulation into 64 consecutive but individual simulation periods with a median length of 9 days. At the start of each of these individual sub-periods, we re-initialized the fractions of water sources by assigning all current water in a mixing cell to the respective initial source area (cf. Figure 3, gray lines). This allowed us to obtain consistent and comparable information on the variation of the mixing of water sources for a total of 64 individual periods across various hydrological conditions. In addition, the separation of the simulation into short sub-periods reduced the possible accumulation of mass balance errors and reset fractions. We chose the sub-periods according to the times at which Glaser et al. (2020) analyzed the simulated surface saturation (Figures 2 and 4) in comparison to the thermal infrared imagery observations. This allowed us to rely on previous simulation output to initialize the hydraulic conditions of the consecutive sub-periods and thus to considerably reduce the wall-clock time of the simulation by running the individual simulation periods in parallel.

3.3. Processing of the HMC Output

With the HMC simulation, we obtained time series for the amount of water originating from the seven predefined source areas and from precipitation at each of the 36 selected POIs. When the mass balance error of the simulated mixing ratio was >5% (i.e., the sum of the individual fractions of water sources of total discharge was <0.95 or >1.05), or when a water fraction was simulated with a negative contribution >1% of simulated discharge, we excluded the affected time step from any further investigations by artificially introducing a gap into the time series of the affected POI (cf. Figure 3).

To identify the delivery processes, that is, the mechanisms that ultimately induce and maintain the occurrence of water at the surface, we analyzed the fractions of water sources after the first time step for each of the 64 sub-period simulations (cf. Figure 3). Since water from one source area is not mixed with water from other source areas within the first time step, the fractions of water sources after the first time step reflect the immediate origin of water entering a mixing cell. Consequently, the HMC output after the first time step allowed us to infer whether the immediate delivery of water to a POI took place via exfiltration from the subsurface, overland flow, or direct precipitation. Based on the assigned source areas (cf. above, Figure 3), we further broke down exfiltration from the subsurface into exfiltration from the fractured bedrock, subsolum, solum, or riparian soil. Overland flow was explicitly separated into overland flow within the stream channel, henceforth referred to as streamflow, overland flow from the hillslopes and plateau, and overland flow from the riparian zone.

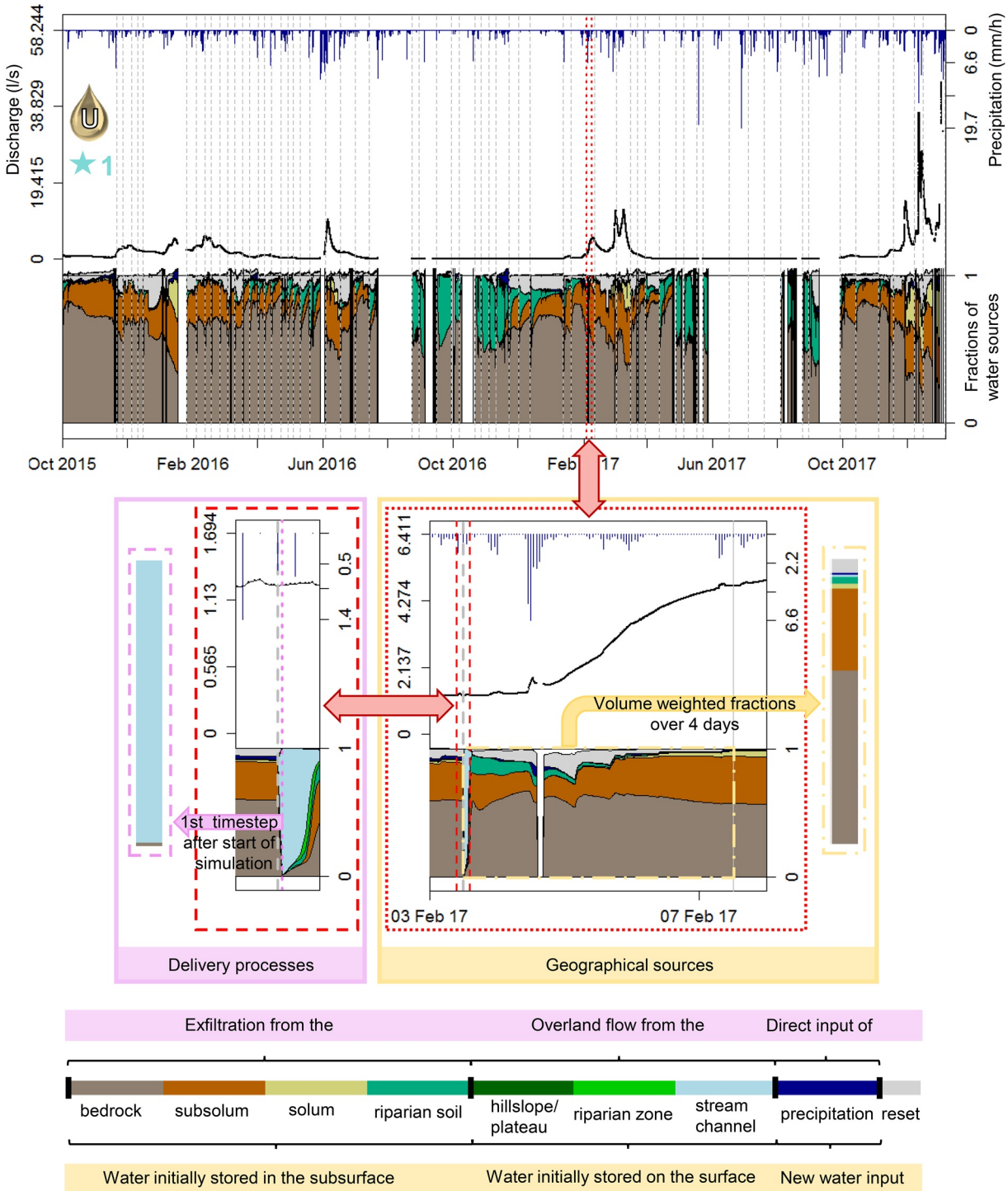

Figure 3. Output and processing of the HMC simulation exemplified for POI 1 located in the stream channel of area *U* (cf. Figure 2). Time series of hourly precipitation and simulated discharge at the POI are shown at the top of each figure panel. Stacked time series for fractions of water originating from the seven different initial source areas defined in the surface and subsurface model domains (cf. Figure 1), fractions of precipitation, and reset fractions visualize the dynamic mixing of water sources (bottom of each figure panel). Gaps in the time series of fractions of water sources indicate that the POI was inactive (simulated discharge is zero) or that the time points were excluded from the analysis due to high mass balance errors (no simulated discharge shown). Gray dotted lines show the start of the 64 simulation sub-periods where water sources were re-initialized according to the seven different source areas.

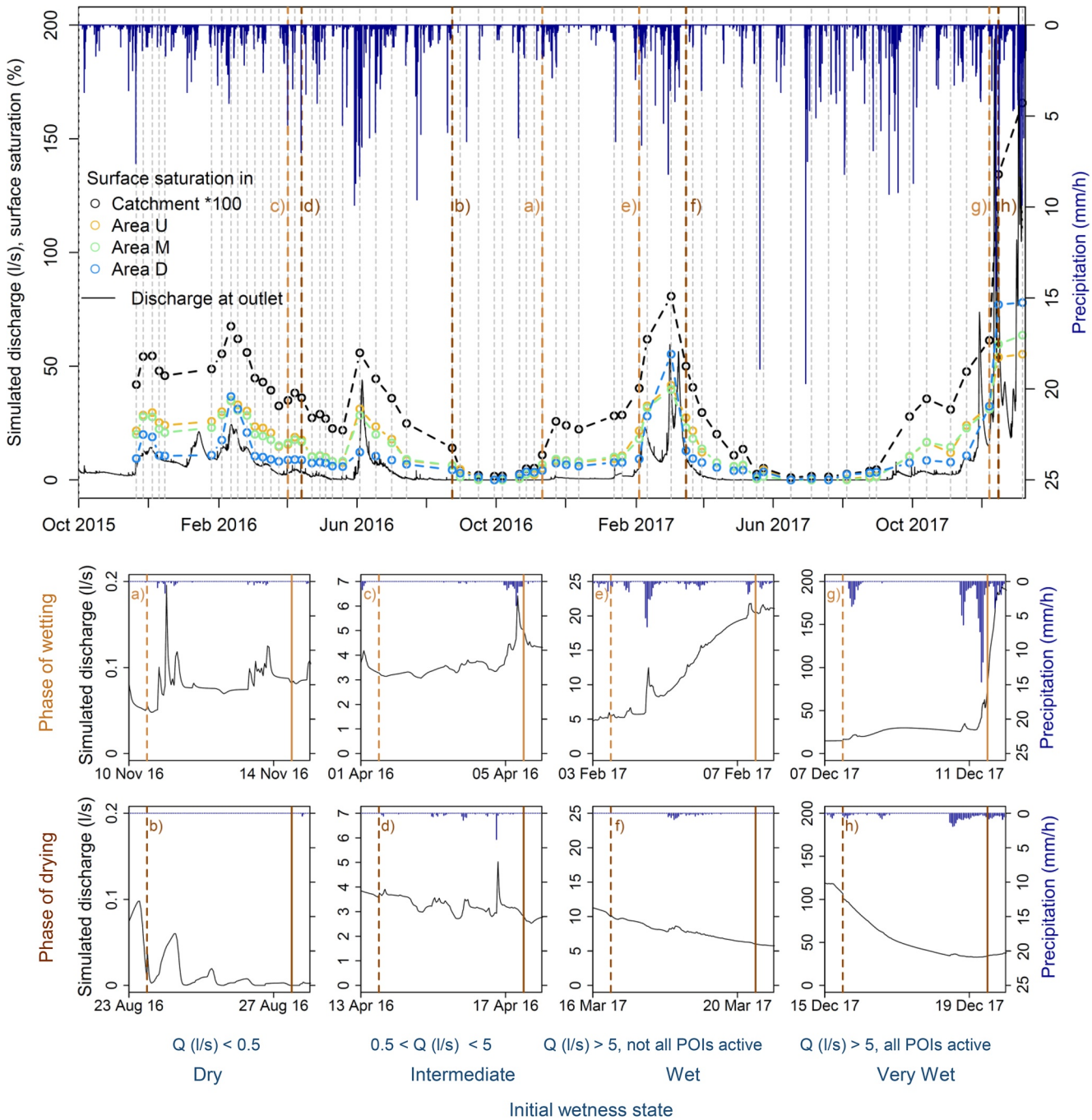

Figure 4. Simulated discharge at the catchment outlet and simulated areal percentage of surface saturation for the entire catchment and for the three riparian-stream areas investigated, *U*, *M*, and *D* (cf. Figures 1 and 2). The areal percentage of surface saturation (water depth $>10^{-4}$ m) was estimated by Glaser et al. (2020) for the times of thermal infrared imagery mapping (cf. Figure 2) and corresponds to the extent of surface saturation at the beginning of the 64 sub-periods of HMC simulation (gray dotted lines, cf. Figure 3). Brown dashed lines, labeled (a–h), mark the beginning and solid lines the end of the eight 4-day periods selected to represent phases of wetting (light brown) and drying (dark brown) starting from different initial wetness states as classified by the simulated discharge *Q* at the catchment outlet.

In order to identify the geographical sources of surface water, that is, the source areas where water was initially stored before reaching a POI, it would be the most intuitive and informative to visually investigate the temporal evolution of the mixing ratio at a POI (cf. Figure 3). Yet it is not feasible to compare the time series of 36 POIs for 64 simulation periods by displaying and analyzing them individually. Instead, we calculated

a summary metric that allows a consistent and reliable comparison of the dominant geographical sources across space and time. This metric is the volume weighted fraction of water sources over the first four days of a simulation period (cf. Figure 3) and we assume it to represent the average mixture of geographical sources at a POI for an inter-event, intra-seasonal time scale. In particular, we distinguished contributions from precipitation, stream channel water, riparian surface water, surface water from the hillslopes and plateau, riparian soil water, water from the solum of the hillslopes and plateau, water from the subsolum, and water from the fractured bedrock (Figure 3). Water from the subsolum and fractured bedrock could indicate contributions from deep subsurface stores from the hillslopes and plateau, as well as contributions from subsurface stores directly underlying the stream channel and riparian soil (for fractured bedrock) and the edges of the riparian zone (for subsolum), respectively (cf. Figure 1). Preliminary assessment at a stream channel POI showed that the closest and the most distant of the predefined source areas (i.e., stream channel vs. solum of the hillslopes and plateau) could occur together in the volume weighted fractions over the first four days of a simulation period (Figure 3 bottom right). We thus decided that–for our study–the time span of four days is a suitable compromise between the fact that water initially stored in adjacent source areas of a POI is displaced by precipitation or by water from more distant sources areas and that water originating from distant source areas needs some time to reach a POI after the start of the simulation.

In total, we obtained 64 different mixing ratios of the delivery processes and geographical sources representing the mixing of water during particular points in time at each of the 36 POIs. In order to assess the spatial variability of the mixing of water sources across the riparian-stream continuum (different categories of POIs, Figure 2) and along the stream (area *U*, *M*, *D*, Figure 1) independently of particular periods in time, we computed for each of the 36 POIs the arithmetic mean of the 64 identified mixing ratios of the delivery processes and geographical sources, respectively. Furthermore, we analyzed the overall time variability of the mixing of water sources across space based on a subset of 8 of the 64 periods, which covered the full range of hydrological conditions commonly occurring within the Weierbach catchment. In particular, we distinguished four categories of initial wetness states: (a) dry, (b) intermediate, (c) wet, and (d) very wet, based on simulated discharge Q at the catchment outlet at the start of the simulated periods: (a) $Q < 0.5$ l/s, (b) 0.5 l/s $< Q <$ 5 l/s, (c) $Q > 5$ l/s with not all POIs active ("active" meaning the existence of surface water at a POI), and (d) $Q > 5$ l/s and all POIs active. Within each of the four categories, we visually selected one simulation sub-period where the simulated catchment discharge Q increased within the first four simulation days and one simulation sub-period where Q decreased within the first four simulation days (Figure 4). Although this selection of a subset of 8 periods was based on catchment discharge Q only, the subset covers phases of wetting and drying within four different wetness categories for all 36 POIs, since discharge dynamics were found to be similar at all POIs and at the catchment outlet (data not shown). Furthermore, the discharge dynamics at the catchment outlet proved to be well correlated to the extent of surface saturation (cf. Figure 4, Glaser et al., 2020). We thus assume that the selected periods represent phases of wetting and drying with increasing and decreasing discharge as well as with expanding and contracting surface saturation across the whole riparian-stream continuum.

4. Results

4.1. Delivery Processes

4.1.1. Time-Averaged Spatial Variability

The dominant process ultimately delivering surface water clearly differed between the stream channel (blue POIs, Figure 5) and the riparian zone (yellow POIs, Figure 5) for all three riparian-stream areas investigated, *U*, *M*, and *D*. Surface water in the stream channel was essentially delivered by overland flow within the stream channel, that is, streamflow that was generated upstream of the study location, while surface water in the riparian zone primarily exfiltrated from the riparian soil. Additional contributions of riparian overland flow to surface saturation were found at most locations in the riparian zone, but the fractions of riparian overland flow varied locally. In the riparian zone of area *U*, one location (POI 6) received surface water nearly exclusively from the riparian soil, while the other POIs showed a higher (POI 9) or even dominant (POI 7) fraction of overland flow. This finding is consistent with conclusions drawn from field observations that distinct locations of groundwater exfiltration exist (cf. Section 2.3, Figure 2). However, in the stream channel of area *U* and within the other two investigated areas, *M* and *D*, POIs positioned at

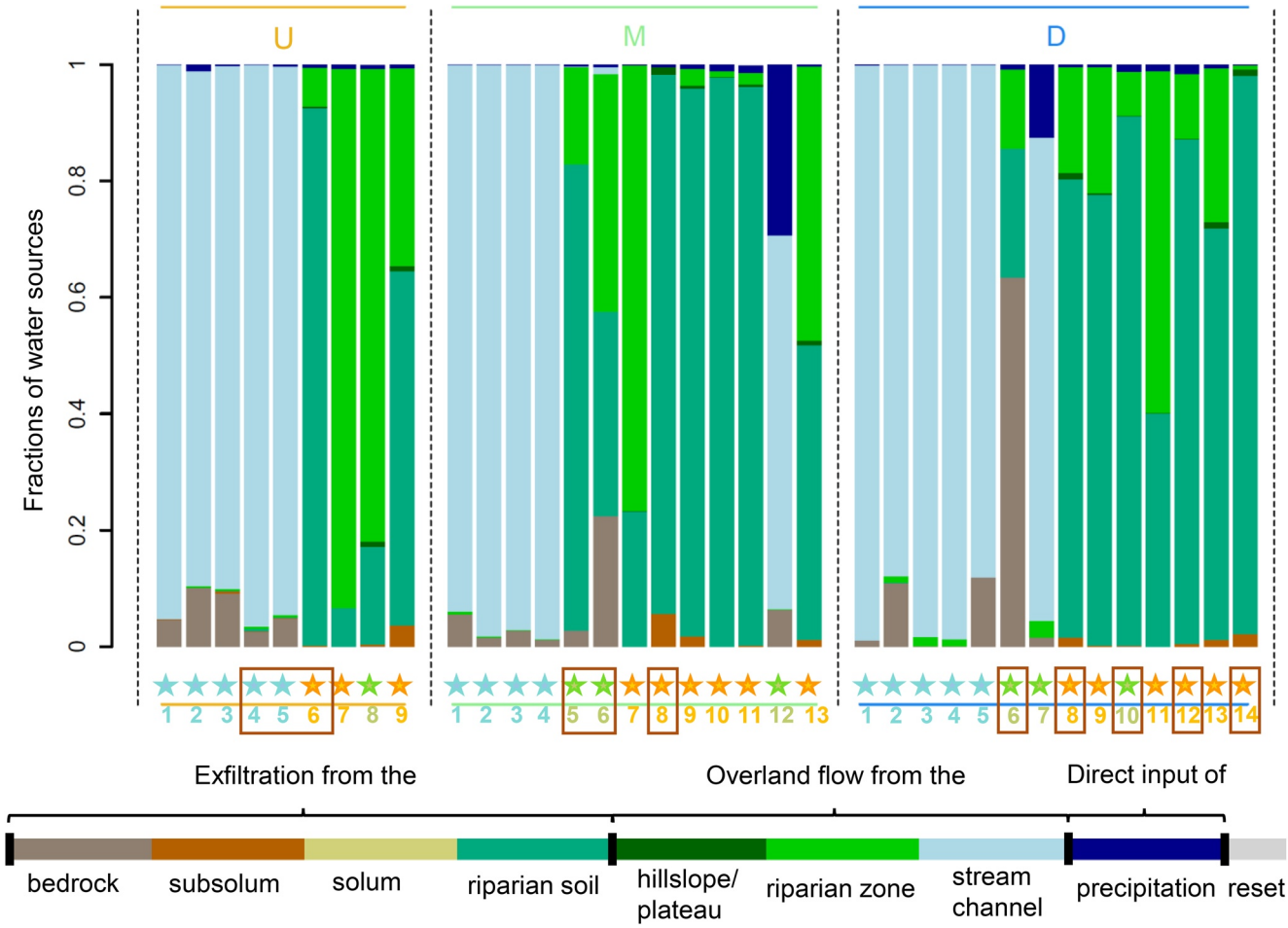

Figure 5. Spatial variability of delivery processes. The bars visualize the mixing ratio of different sources of surface water at the 36 POIs located in the stream channel (blue stars), in the riparian zone (yellow stars), and at unclassifiable positions (green stars) in areas *U*, *M*, and *D* (cf. Figure 2). The POIs enclosed in brown boxes are at locations with assumed distinct exfiltration of subsurface water (cf. Figure 2). The fractions of water sources are the arithmetic mean of the fractions of water sources after the first time step of each of the 64 sub-period simulations (cf. Figure 3).

locations that were assumed to be predominantly fed by groundwater exfiltration (POIs enclosed in brown boxes in Figure 5) did not show distinctly different delivery processes for surface water than other locations in the riparian zone and stream channel, respectively. POIs that could not be clearly assigned to the stream channel or riparian zone based on their location and saturation frequency (Figure 5, green POIs) mostly showed similar delivery processes as found for the locations in the riparian zone. Exceptions are POI 6 in area *D*, where the dominant delivery process was exfiltration from the fractured bedrock, and POI 7 in area *D* and POI 12 in area *M* that were the only two POIs showing a marked delivery of surface water via direct precipitation.

4.1.2. Temporal Variability

The dominant delivery processes did not change substantially between differing initial wetness states and phases of drying and wetting (Figure 6). The largest temporal variation at stream channel locations occurred between periods with dry and intermediate initial wetness (Figures 6a–6d, blue POIs): the fraction of water exfiltrating from the bedrock was considerably higher during periods with dry initial conditions than with intermediate initial conditions, especially during the wetting phase (Figure 6a). At the riparian POIs and most unclassified locations, the mixing ratio of the delivery processes remained stable once the delivery of water to the surface was activated (Figure 6, yellow and green POIs). Only during drying after very wet initial conditions (Figure 6h), the fraction of overland flow was considerably increased relative to the exfiltration of subsurface water, and overland flow and exfiltrating subsurface water partly originated from

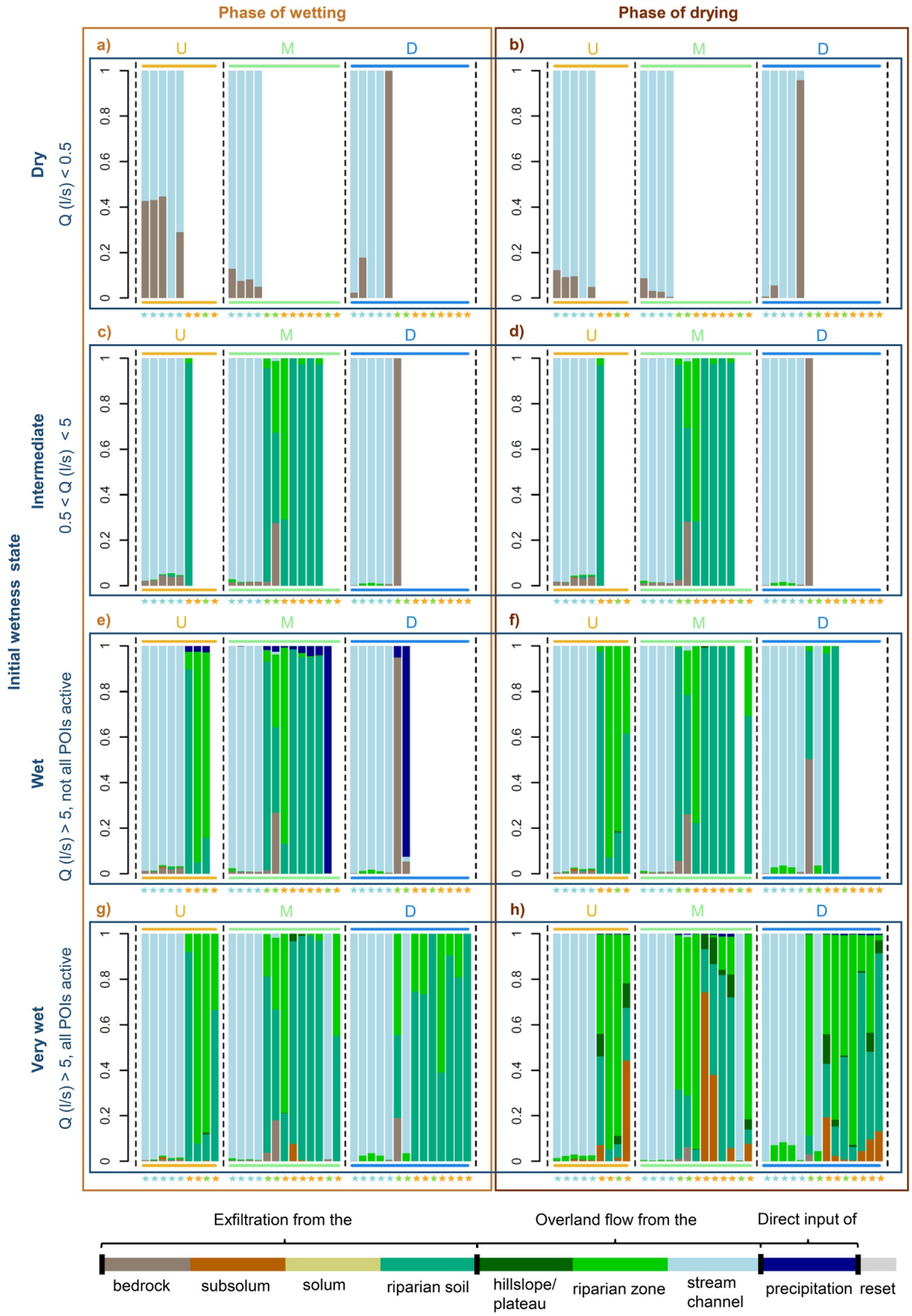

Figure 6. Temporal variability of delivery processes depending on the initial wetness state and phases of wetting or drying. The bars visualize the mixing ratio of sources for surface water after the first time step (cf. Figure 3) for each of the eight selected periods (a–h), Figure 4) at the 36 POIs located in the stream channel (blue stars), in the riparian zone (yellow stars), and at unclassifiable positions (green stars) in areas *U*, *M*, and *D* (cf. Figure 2). Missing bars indicate that the POI was inactive (no discharge simulated) within the first time step.

more distant source areas (i.e., hillslopes/plateau and subsolum). Exceptionally high temporal variability with substantial changes in the dominant delivery processes with increasing wetness occurred at the three POIs at unclassified locations that showed differing dominant delivery processes in general (POI 6 and 7 in area *D*, POI 12 in area *M*, cf. Section 4.1.1).

Precipitation occurred within the first time step and thus as an identifiable delivery process (cf. Section 3.3) for the selected simulation periods e and h (cf. Figure 4). Nonetheless, contributions of direct precipitation to the delivery of surface water were only found at non-stream locations (green and yellow POIs, Figure 6) and the fractions were minor (period e) to negligible (period h) compared to the fractions of overland flow and exfiltration from the subsurface. Exceptions are again POI 12 in area *M* and POI 6 in area *D*, where precipitation clearly dominated the delivery of surface water at the beginning of simulation period e (Figure 6e), but also became negligible compared to other delivery processes (in this case inundation by streamflow) for the very wet conditions of period h (Figure 6h).

4.2. Geographical Sources

4.2.1. Time-Averaged Spatial Variability

The most apparent spatial variability in the time-averaged mixing ratio of geographical sources of surface water (Figure 7) was that stream channel water was found exclusively at stream channel locations (including POI 12 in area *M*, POI 7 in area *D*, cf. Section 4.1). Apart from that, the geographical sources of surface water were similar across the riparian-stream continuum and water that was initially stored in the subsurface clearly dominated over water from surface source areas and newly incoming precipitation (except POI 12 in area *M*, POI 7 in area *D*). The dominance of subsurface water clearly matched the identified dominant delivery of surface water via exfiltration in the riparian zone (cf. Section 4.1), but it initially seemed contradictory to the dominant delivery via streamflow at stream channel locations. However, the minor fractions of exfiltration from the bedrock as a delivery process at the stream channel locations do not necessarily imply that the exfiltration of subsurface water ceased with increasing wetness (cf. Figure 6), but rather that its contribution became less relevant in comparison to streamflow generated upstream of the study locations. Thus, the apparent discrepancy between delivery processes and geographical sources at stream channel locations can be resolved by streamflow being generated by subsurface water exfiltrating all along the stream channel and accumulating downstream. Increasing fractions of water initially stored in the stream channel in the downstream direction (area $U < M < D$, Figure 7) and the appearance of exfiltration from the bedrock as a relevant delivery process during dry conditions all along the stream channel (Figures 6a and 6b) substantiate this process description.

Local variations in the mixing ratio of water from different subsurface stores occurred along the stream channel (higher fraction of subsolum water relative to riparian soil water in area *U* than in areas *M* and *D*), between the stream channel and the riparian zone (tendentially smaller fractions of riparian soil water at stream channel locations), and within the riparian zone (varying fractions of water from the fractured bedrock and riparian soil). Moreover, the fractions of precipitation water were slightly higher at POIs in the stream channel than at POIs in the riparian zone, especially in area *M*. However, the reset fraction and thus the fraction of unknown water origin (cf. Section 3.1) at many locations was higher than the fraction of precipitation. These proportionally high reset fractions hamper interpretations of the spatial distribution of the contribution of precipitation water and other geographical water sources with small or non-existing fractions (e.g., riparian surface water).

4.2.2. Temporal Variability

The mixing ratios of the geographical sources of surface water clearly differed between wetting and drying phases regarding the contribution of precipitation water (Figure 8). The fractions of precipitation were very minor during the selected drying phases, whereas they were still small but more marked during the selected wetting phases. An exception was a similar relative contribution of precipitation to surface water during both the wetting and drying period with intermediate initial wetness conditions (Figures 8c and 8d). It should be noted that the cumulative amount of precipitation was similar for these two periods c and d, while it clearly differed between the wetting and drying phases of the other initial wetness conditions (cf. Figure 4). Thus, it is likely that the differences identified in the fractions of precipitation between the

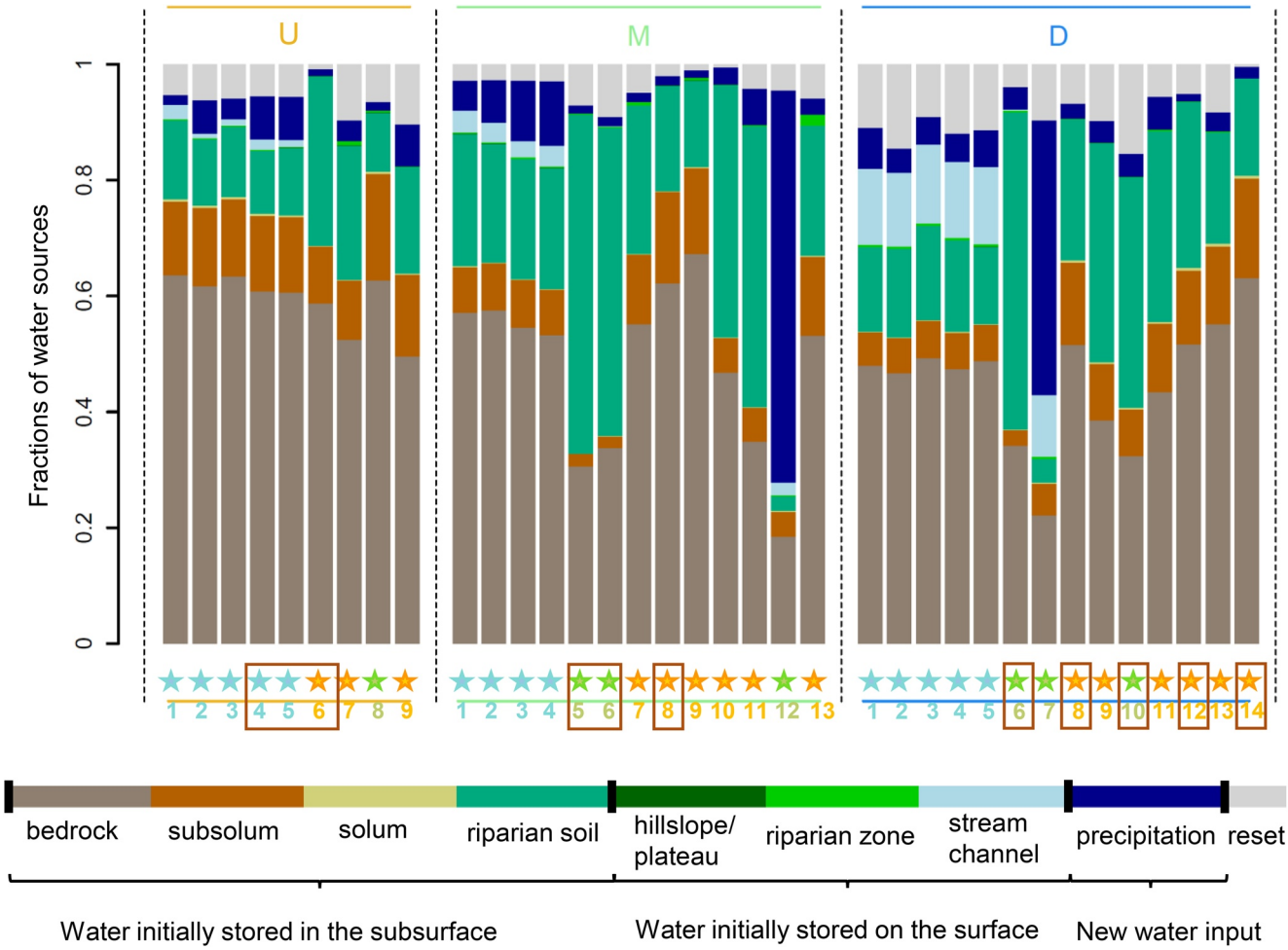

Figure 7. Spatial variability of geographical sources. The bars visualize the mixing ratio of different sources for surface water at the 36 POIs located in the stream channel (blue stars), in the riparian zone (yellow stars), and at unclassifiable positions (green stars) in areas *U*, *M*, and *D* (cf. Figure 2). The POIs enclosed in brown boxes are at locations with assumed distinct exfiltration of subsurface water (cf. Figure 2). The fractions of water sources are the arithmetic mean of the volume weighted fractions of the first four days (cf. Figure 3) of each of the 64 sub-period simulations.

investigated periods relate to the amount of precipitation in relation to discharge rather than to a simple distinction between wetting and drying. The fractions of the other geographical water sources differed between the selected phases of wetting and drying in some areas or for some initial wetness states. However, we did not find any indications of clearly and systematically different geographical sources of surface water between the phases of wetting and drying, which is similar to the findings for the delivery processes (cf. Section 4.1).

In contrast, the initial wetness state clearly influenced the mixing ratios of the geographical sources of surface water. At stream channel locations (Figure 8, blue POIs), surface water mainly originated from the riparian soil and fractured bedrock for dry initial conditions (Figures 8a and 8b), subsolum water appeared as a clear contributor with intermediate initial wetness conditions (Figures 8c and 8d), and the mixing ratio between riparian soil water and subsolum water shifted towards higher contributions of subsolum water with increasing wetness (Figures 8c–8h). In addition, contributions of water initially stored in the stream channel were highest for intermediate wetness, and considerable fractions of solum water appeared during wet conditions (especially in area *U*, Figures 8e–8h). In the riparian zone and at unclassified locations (Figure 8, yellow and green POIs), the mixing ratio of geographical sources mainly shifted to smaller fractions of riparian soil water in favor of higher fractions of subsolum water with increasing wetness. At the exceptional POIs 12 in area *M* and 7 in area *D* (cf. Section 4.1), the geographical sources changed completely from nearly exclusive contributions of precipitation water (Figures 8a–8d) to a mixture of subsurface sources

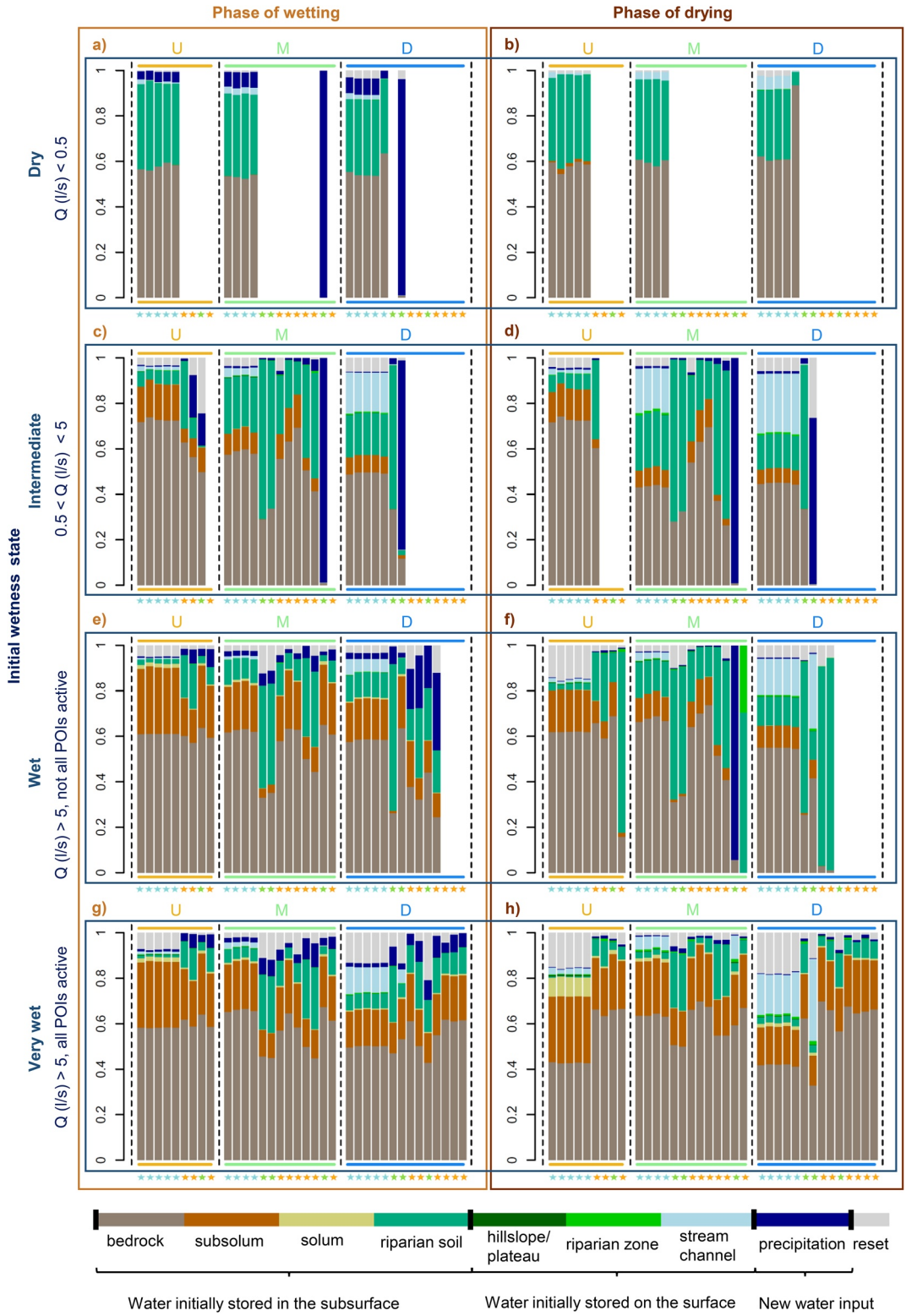

Figure 8. Temporal variability of geographical sources depending on the initial wetness state and phases of wetting or drying. The bars visualize the mixing ratio of the volume weighted fractions of water sources of the first four days (cf. Figure 3) for each of the eight selected periods (a–h), Figure 4) at the 36 POIs located in the stream channel (blue stars), in the riparian zone (yellow stars), and at unclassifiable positions (green stars) in areas *U*, *M*, and *D* (cf. Figure 2). Missing bars indicate that the POI was inactive (no discharge simulated) over all four days.

similar to that found in the stream channel (Figures 8e–8h), reflecting the switch of the delivery of surface water from precipitation to streamflow identified for these two POIs (cf. Figure 6).

5. Discussion

Our simulation results show that ISSHM HMC modeling can provide very detailed and differentiated information on the spatial and temporal variability of sources of surface water in the riparian-stream continuum of an intermittent stream. The application of the HMC modeling at an extensively studied test site further allowed us to recognize the extent to which comprehensively validated simulations can be an asset in the planning and interpretation of time-consuming and costly field studies (see Section 5.2). The focus of our study was to compare the mixing ratio of various water sources between different locations, initial wetness states, and phases of wetting and drying. We achieved this through a novel approach for processing and displaying the HMC simulation results, which goes beyond previous studies (e.g., Berezowski et al., 2019; Gutiérrez-Jurado et al., 2019; Partington et al., 2013). In the following paragraphs, we discuss this data processing and the information obtained (Section 5.1) and demonstrate how the approach can enhance our understanding of the spatio-temporal generation of riparian surface saturation and streamflow, using the example of the Weierbach catchment (Section 5.2). It was not within the scope of this study to decipher the water sources at event-scale, yet it should be noted here that a different way of analyzing the hourly-resolved simulation results would allow such investigations, for example, by explicitly analyzing the sub-daily evolution of the time series of water fractions (cf. Figure 3) for distinct locations and events.

5.1. Identification of Water Sources With the Hydraulic Mixing-Cell Approach

In order to obtain a comprehensive picture of the varying sources of surface water in space and time with the HMC approach, we (a) distinguished different initial source areas for the surface and—for the first time—also for the subsurface domain and (b) accomplished a clear conceptual separation between delivery processes and geographical sources. The latter was achieved by analyzing the mixing of water after the first time step and from volume weighted fractions over the first four days, respectively. This approach requires a simulation to be split into sub-periods when seeking the temporal change of mixing ratios and is not suited to analyzing the temporal change of water sources within the short time-scale of single rainfall-runoff events. Moreover, applying different time interval criteria for the analysis of the delivery processes and geographical sources would result in partly different mixing ratios. Our approach is thus not appropriate to unambiguously quantify the contribution of single delivery paths and geographical sources. Yet our results corroborate that our approach was highly valuable to reveal the relative importance of different delivery paths and geographical source areas at different locations and to summarize the overall temporal variability of this relative importance at an inter-event, intra-seasonal time scale–consistently to a visual assessment of the full time series (cf. Figures 3 and 8). We therefore think that any uncertainty in the identified mixing ratios due to the selection of particular time interval criteria can be considered minor for comparing the dominant water sources between different locations, initial wetness states, and phases of wetting and drying as long as the same criteria are applied for all locations and periods of investigation. Since we defined our periods of investigation based on the availability of thermal infrared observations and previous model output analyses (cf. Section 3.2, Glaser et al., 2020), we cannot currently provide a systematic analysis of the water sources as a function of precipitation amount and its ratio to discharge volume (cf. Section 4.2.2, Figure 8). Still, the often dominant contribution of precipitation to surface water at POI 12 in area *M* and POI 7 in area *D* (cf. Section 4.1.2 and 4.2.2) demonstrates that the small contribution of precipitation observed at all other POIs is not an artefact of the characteristics of the selected periods or the selected time interval criteria. Thus, a comparison of the water sources at different locations and times is also possible for the contribution of precipitation and we deem our new approach highly valuable for studying water fluxes in the river corridor and streamflow generation.

The presented approach can in principle be applied at any other study site, but it may be necessary to adapt the here chosen time interval criteria according to the local system characteristics and the specific aims of the study. This is especially the case for the identification of the geographical sources. We selected a time span of four days as an appropriate value for our study site and investigations, since a preliminary assessment of the HMC results showed the four days to allow water from all predefined sources to reach a POI and

to not overrate nor completely eliminate the signal of close-by source areas, where initially stored water is flushed out within few hours or days after each re-initialization (e.g., stream channel water, riparian water, cf. Figure 3, Section 3.3). Longer time spans are likely needed to achieve a similar compromise for study sites with larger and more distant source areas or slower flow paths, yet this also depends on the research objectives. Similarly, four days would likely not be sufficient to capture all possible water sources if we further differentiated our predefined source area "bedrock" into "bedrock below stream channel and riparian zone" and "bedrock below hillslope and plateau". This circumstance reflects a general problem when investigating geographical sources, namely that the results always depend on a study-specific and somehow arbitrary definition of distinct source areas. An important aspect to consider here is that every definition of a geographical source area must entail a reference state and time that determines whether water is considered to originate from the particular source area (since all water must have entered the source area at some point via precipitation or from another source area), but that these criteria are commonly only considered implicitly (e.g., based on where and when end members are sampled for end member mixing analyses). In that regard, our approach of analyzing the volume weighted fractions over a certain time span has the advantage that this initial state and reference time are defined explicitly and thus are easy to adapt and to be defined identically for all analyzed geographical sources. It facilitates to target the analysis to a specific question, helps to interpret the identified sources, and allows a consistent comparison of the importance of various predefined source areas at different locations and moments in time. For example, a particular short time span could be chosen in a future study to compare the dominant geographical sources in different rainfall-runoff events, explicitly focusing on fast connecting source areas and ignoring distant source areas with long travel times.

The main challenge for the application of the HMC approach were numerical issues resulting in reset fractions, that is, the fractions of water with unknown origin (cf. Section 3.1). The reset fractions are required to avoid mass balance errors in the mixing calculation due to numerical instability or numerical dispersion, but they introduce uncertainties in the mixing ratios. Partington et al. (2013) suggested accepting reset fractions <1%. They pointed out that the numerical stability of the HMC approach is particularly critical for mixing cells whose water storage volume is relatively small compared to volumetric fluxes of water inflow and outflow. While such situations were not reported to cause problems in other HMC studies on water sources in floodplains and intermittent streams (Berezowski et al., 2019; Gutiérrez-Jurado et al., 2019; Partington et al., 2013), they tended to occur for our simulations because of a large variability in the presence of surface water and shallow surface water depths in the highly-resolved mesh of the riparian zone and stream channel. We managed to limit the reset fractions and mass balance errors by using hourly input data, splitting the total simulation period of 28 months into sub-periods with a median length of 9 days (cf. Section 3.2), and relaxing some numerical stability criteria. However, we could not minimize the reset fractions to values <1% for stable simulations with reasonable calculation times. At various locations within the model domain, our adaptations were not sufficient to obtain reliable simulation results (data not shown) and further adaptations of the model setup (e.g., mesh setup) and the HMC code itself (e.g., stability criteria) might help to overcome these current limitations. A promising approach to achieve such further improvements could be to rely on the experience with similar numerical issues occurring in the context of modeling solute transport.

Nonetheless, for the locations and periods that we investigated in this study, mass balance errors and the extent of reset fractions were kept within reasonable limits, that is, the median removal of simulation results at the 36 POIs due to mass balance errors (cf. gaps in Figure 3) was 1% for the analyzed $64 \times 4 = 256$ days (maximum removals of 2.7% and 4.4% at POI 2 in area *U*, POI 12 in area *M*, <0.01% removals at POI 10 in area *M* and POI 13, 14 in area *D*) and the median percentage with reset fractions >10% was 2.6% of the analyzed 256 days (maximum values of 23.5% and 28.5% at POI 3 and 2 in area *U*, values <0.05% at POI 2, 8, 10 in area *M*). During the periods with reset fractions similar to or higher than fractions of other sources, the mixing ratio of the water sources might be considerably distorted if all water that was assigned with reset fractions originated from the same initial source, for example, precipitation. However, we did not find signs of obvious distortion and it is unlikely that the reset fraction represents only one initial water source. We are therefore confident that the information obtained on the mixing ratio of the water sources is robust and allows the relevance of different water sources and their spatial and temporal variability to be inferred. Future research may target a combined use of the HMC approach with solute transport modeling and

particle tracking to profit from the advantages of the different approaches and thus reduce method-specific limitations and further strengthen the robustness of the information on the water sources.

5.2. Insights From the HMC Modeling on Sources of Surface Water in Comparison to Previous Experimental and Simulation Studies at the Study Site and Beyond

5.2.1. Spatial Variability of Water Sources

Previous studies in the Weierbach catchment suggested that surface saturation in the riparian zone is largely induced and sustained by groundwater that exfiltrates at discrete locations (cf. Figure 2) and distributes across the riparian zone via overland flow (Antonelli et al., 2020a, 2020b; Glaser et al., 2018, 2020). The HMC simulation confirmed the high relevance of subsurface water sources and specified that large fractions of the riparian surface water were initially stored in the riparian soil and fractured bedrock (Figures 7 and 8). However, the model did not only reproduce an exfiltration of subsurface water at the locally confined locations identified with thermal infrared imagery (cf. Section 2.3, Figure 2). It also simulated exfiltration ubiquitously across the riparian zone (cf. Section 4.1.1) whereas overland flow from adjacent model elements only exceeded the delivery of surface water via exfiltration at a few of the riparian POIs (Figures 5 and 6). Moreover, the model did not simulate any relevant expansion of streamflow into the riparian zone, not even at the riparian-stream interface (cf. green POIs Figures 5–8, except POI 12 in area *M*, POI 7 in area *D*), which differs from previous process descriptions based on thermal infrared imagery mapping (cf. Section 2.3, Antonelli et al., 2020a; Glaser et al., 2018)). Nonetheless, the model results do not contradict field observations since the field-based expectations of a more heterogeneous delivery of surface water than subsurface water exfiltration were mostly based on the heterogeneous patterns and frequencies of surface saturation (cf. Section 2.3) that were largely reproduced with the simulations (cf. Figure 2, Glaser et al., 2020). This clearly demonstrates the asset of HMC simulations in complementing the interpretation of field observations when model realism is assured. In a next step, the results of the HMC analysis could be further tested by measurements of geochemistry or isotope data to identify the water sources (cf. Berezowski et al., 2019; Schilling et al., 2017) and likewise, could help to select the most interesting locations with exceptional sources (e.g., POI 12, area *M*, POI 7, area *D*) for further detailed sampling campaigns.

The spatial differentiation between the stream channel and riparian zone became particularly obvious from the conceptual separation between delivery processes and geographical sources. Without the information on the delivery processes (Figures 5 and 6), no spatial difference between the stream channel (dominant delivery of surface water via streamflow generated upstream) and riparian zone (dominant delivery of surface water via in-situ exfiltration of subsurface water) would have been identified. Without the information on the geographical sources (Figures 7 and 8), the actual sources of stream water "generated upstream" would have remained unclear. Only by combining the information on the delivery processes and geographical sources was it possible to infer that streamflow was generated by subsurface water exfiltrating all along the stream channel and accumulating downstream. The identified similarity of geographical sources of surface water in the stream channel and riparian zone (Figures 7 and 8) further suggests that overland flow in the riparian zone (cf. POIs in the riparian zone, Figure 5) is basically intermittent streamflow generated by the exfiltration of subsurface water outside of the visually apparent stream channel. Although direct contributions of overland flow from the adjacent riparian zone to stream channel water were minor compared to streamflow generated upstream (Figures 5 and 6), it is possible that most of the riparian surface water eventually entered the stream channel via overland flow. Further analyses with the HMC approach similar to Partington et al. (2013) and Gutiérrez-Jurado et al. (2019) could help to quantify both the fraction of water in the stream channel that actually passed through the riparian zone as overland flow, and the active contribution of riparian surface saturation to streamflow in comparison with the actual extent of surface saturation.

Overall, the sources of stream water and riparian surface water were homogeneous within and among the riparian-stream areas investigated in the Weierbach catchment compared to the heterogeneous frequencies of surface saturation observed and simulated (cf. Figure 2), results from other studies simulating the generation of surface saturation across space (Berezowski et al., 2019; Partington et al., 2013; Weill et al., 2013), and the variability of stream water sources found in catchments with varying landscape characteristics (e.g., Cowie et al., 2017; Gordon et al., 2015; Laudon et al., 2007). Further HMC studies analyzing the sources

of surface water in riparian-stream continua and floodplains in different, larger, and more heterogeneous landscapes compared to the forested, humid-temperate Weierbach catchment may help to clarify what controls the dominance of a certain process, for example, subsurface water exfiltration versus stream inundation (e.g., Berezowski et al., 2019; Bonnet et al., 2017), and the degree of the spatial variability of water sources. Yet, even the small spatial variabilities in the sources of riparian surface water and stream water identified in the Weierbach catchment (cf. Section 4.1.1, 4.2.1) may be relevant. For example, the spatially varying importance of overland flow (Figure 5) and riparian soil water relative to other subsurface sources (Figure 7) for riparian surface water might already be sufficient to create hot spots of biogeochemical and ecological activity as often identified in riparian zones and floodplains (Frei et al., 2012; Grabs et al., 2012; Harms & Grimm, 2008; Krause et al., 2017; Ramey & Richardson, 2017; Singer et al., 2016). Furthermore, the small spatial variabilities of geographical water sources may also impact the representativeness of water samples for water quality analyses or end member mixing analyses. The spatial difference of the simulated water sources was not related to any visually apparent criteria such as saturation frequency, saturation persistence, locations of obvious groundwater exfiltration, or distance to the stream. This implies that these criteria may not guarantee a selection of representative sampling locations. Instead, HMC simulations could be a useful tool to support the selection of representative water sampling locations.

5.2.2. Temporal Variability of Water Sources

The contributions of precipitation to surface water were always minor compared to those of subsurface water at 34 out of the 36 POIs (cf. Figure 8). Even during periods of wetting where simulated discharge volume clearly reacted to precipitation events (cf. Figure 4), the simulated increase of discharge volume largely related to an increased exfiltration of subsurface water, most likely triggered by increased pressure gradients and an expansion of subsurface saturation induced by infiltrating precipitation. This finding demonstrates that ISSHMs such as HGS can reproduce the often observed phenomenon of a fast release of previously stored subsurface water to the stream as an immediate response to precipitation (e.g., Cartwright & Morgenstern, 2018; Correa et al., 2019; Kirchner, 2003; Laudon et al., 2007). The importance of a precipitation-induced expansion of subsurface saturation and the subsequent exfiltration of subsurface water is also consistent with the variable source area concept for forested humid catchments (e.g., Dunne & Black, 1970; Hewlett & Hibbert, 1967; Megahan & King, 1985) and with previous tracer studies in the Weierbach catchment that revealed old water stored in the subsurface to be the main contributor to streamflow (Martinez-Carreras et al., 2015; Rodriguez & Klaus, 2019; Wrede et al., 2015). However, both the variable source area concept and previous studies in the Weierbach catchment (Fenicia et al., 2014; Glaser et al., 2016; Klaus et al., 2015; Martinez-Carreras et al., 2015, 2016; Rodriguez & Klaus, 2019; Wrede et al., 2015) presume and emphasize relevant contributions of precipitation to event surface water. Future work is needed to analyze the hourly HMC simulation results with an explicit focus on the intra-event-scale (cf. Section 5.0) to quantify and evaluate the simulated contribution of precipitation during distinct rainfall-runoff events, including the characteristic sharp, short-lasting first discharge peaks in the Weierbach catchment (cf. Section 2.1, Figures 3 and 4) where precipitation was found to represent up to 60% of the hydrograph (Martinez-Carreras et al., 2015).

The sources of surface water were rather unaffected by precipitation and phases of wetting or drying, but the geographical water sources clearly varied depending on the initial wetness state (Section 4.2.2). In particular, the consideration of several subsurface source areas revealed a gradual activation of additional upslope source areas and upper soil layers by an increasing extent of subsurface saturation with increasing wetness. The identified shift in stream water sources from high fractions of riparian soil water to high fractions of water stored in the subsolum and solum (Figure 8) complements findings from previous hydrograph separations in the Weierbach catchment that revealed a less dominant contribution of riparian soil water to runoff events during wetter conditions (Martinez-Carreras et al., 2015). It is also in line with tracer studies in other catchments that highlighted that the activation of high streamflow was related to an initiation and connection of hillslope runoff (Correa et al., 2017; McGlynn & McDonnell, 2003) and shallow interflow from soils or regolith (Cartwright & Morgenstern, 2018; Correa et al., 2017), whereas low flow largely consisted of water stored in the riparian soil (Correa et al., 2017; McGlynn & McDonnell, 2003), spring water from underlying bedrock (Correa et al., 2017), and groundwater (Cartwright & Morgenstern, 2018). Furthermore, the highest contribution of water initially stored in the stream channel at intermediate wetness (Figure 8) suggests that an increase of streamflow from dry to intermediate conditions was related to a considerable

increase of active stream length, induced by an upstream expansion of subsurface saturation (cf. Hewlett & Hibbert, 1967). Only once intermittent streamflow was activated all along the stream channel and discharge volume further increased without a further increase of active stream length (cf. Antonelli et al., 2020b), did contributions from additional, more distant subsurface stores than riparian soil and fractured bedrock underlying the stream channel become more relevant (Figures 8e–8h).

The increase of active POIs and fractions of subsolum water with increasing wetness in the riparian zone (Figure 8) implies that locations of exfiltration expanded with increasing wetness towards the edges of the riparian zone (underlain by subsolum, cf. Figure 2), which subsequently leads to an increased extent of riparian surface saturation and riparian overland flow (cf. Figures 6a and 6b). This process description matches the perceptual model on the expansion of surface saturation in the riparian zone of the Weierbach catchment derived from the thermal infrared imagery mapping of the spatio-temporal variability of surface saturation (Antonelli et al., 2020a). Yet the HMC results do not support the field-derived perception that riparian surface saturation persists during drying phases solely due to a low infiltration capacity of the riparian soil and overland flow from neighboring areas. Instead, we identified a continued exfiltration of subsurface water to the surface during drying phases and identified a distinct shift of the mixing ratio from exfiltration to overland flow between wetting to drying for very wet initial conditions only (Figure 6). In conclusion, the process understanding gained from the temporal variability of simulated water sources and its consistency and enhancement in comparison to previous findings from various laborious field studies within and beyond the Weierbach catchment demonstrate once more the value of using HMC simulations to complement time and cost-intensive field sampling campaigns to obtain a comprehensive understanding of varying flow paths and water sources.

6. Conclusions

We investigated the sources of surface water and their variability in space and time using a hydraulic mixing-cell approach in a comprehensively validated HydroGeoSphere model. We introduced a novel approach of employing the hydraulic mixing-cell simulation that allowed us to specify and quantify the mechanisms that induce and maintain the occurrence of surface water (i.e., delivery processes) and the geographical sources of surface water, including three different surface areas and four different subsurface stores. The information obtained from the HMC simulation goes beyond standard model output and was very valuable for identifying and comparing the contributions of various sources of surface water at different locations across the riparian stream-continuum and for varying initial wetness conditions and phases of wetting and drying. Furthermore, the HMC modeling supported, clarified, and enhanced the understanding from previous investigations in the Weierbach catchment, our exemplary study site. In particular, the HMC results confirmed previous perceptions on the important role of subsurface water for the generation of riparian surface saturation and intermittent streamflow. In addition, the HMC simulation revealed a varying contribution of different subsurface stores, pointing to a gradual activation of upslope source areas, in addition to the riparian soil and fractured bedrock underlying the stream channel, by increasing wetness. The spatial variability of the delivery processes and geographical sources of surface water was found to be smaller than expected from the heterogeneous patterns and frequencies of surface saturation observed and simulated in the riparian-stream continuum of the Weierbach catchment. Yet we still identified some spatial variations in the water sources that may be relevant for point-sampling, hotspots of biogeochemical activity, or microhabitats. Lastly, the sources of surface water were rather stable between phases of wetting and drying, and contributions of riparian overland flow and precipitation were generally small. Future analyses of the hourly-resolved simulation results may further clarify whether contributions of precipitation and riparian overland flow to surface water were also minor throughout single rainfall-runoff events and if and how much riparian surface saturation eventually connected to the stream. Moving beyond our exemplary study site, we (a) encourage using HMC modeling as a complement to field data, either to help interpret and understand the field data or to plan experiments beforehand; and (b) wish to motivate similar studies on the sources of surface water in other riparian-stream continua and floodplains to understand how the processes and spatial and temporal variability identified for the Weierbach catchment relate to specific landscape characteristics such as area and stream size, climatic conditions, or subsurface properties.

Conflict of Interest

The authors declare no conflicts of interest relevant to this study.

Data Availability Statement

The hourly-resolved meteorological forcing data and HMC simulation results are available at https://doi.org/10.5281/zenodo.4700426

Acknowledgments
Barbara Glaser and Julian Klaus thank the Luxembourg National Research Fund (FNR) for funding within the framework of the FNR-AFR Pathfinder project (ID 10189601).

References

Antonelli, M., Glaser, B., Teuling, A. J., Klaus, J., & Pfister, L. (2020a). Saturated areas through the lens: 1. Spatio-temporal variability of surface saturation documented through thermal infrared imagery. *Hydrological Processes*, *34*(6), 1310–1332. https://doi.org/10.1002/hyp.13698

Antonelli, M., Glaser, B., Teuling, A. J., Klaus, J., & Pfister, L. (2020b). Saturated areas through the lens: 2. Spatio-temporal variability of streamflow generation and its relationship with surface saturation. *Hydrological Processes*, *34*(6), 1333–1349. https://doi.org/10.1002/hyp.13607

Aquanty Inc. (2018). *HGS user manual*. Retrieved from https://static1.squarespace.com/static/54611cc8e4b0f88a2c1abc57/t/5e39cd-761c3ae5719bca385c/1580846461934/hydrosphere_user.pdf

Barthold, F. K., & Woods, R. A. (2015). Stormflow generation: A meta-analysis of field evidence from small, forested catchments. *Water Resources Research*, *51*, 3730–3753. https://doi.org/10.1002/2014WR016221

Berezowski, T., Partington, D., Chormański, J., & Batelaan, O. (2019). Spatiotemporal dynamics of the active perirheic zone in a natural wetland floodplain. *Water Resources Research*, *55*(11), 9544–9562. https://doi.org/10.1029/2019WR024777

Berg, S. J., & Sudicky, E. A. (2019). Toward large-scale integrated surface and subsurface modeling. *Groundwater*, *57*(1), 1–2. https://doi.org/10.1111/gwat.12844

Beumer, V., Van Wirdum, G., Beltman, B., Griffioen, J., & Verhoeven, J. T. A. (2007). Biogeochemical consequences of winter flooding in brook valleys. *Biogeochemistry*, *86*(1), 105–121. https://doi.org/10.1007/s10533-007-9150-y

Birkel, C., Soulsby, C., Tetzlaff, D., Dunn, S., & Spezia, L. (2012). High-frequency storm event isotope sampling reveals time-variant transit time distributions and influence of diurnal cycles. *Hydrological Processes*, *26*(2), 308–316. https://doi.org/10.1002/hyp.8210

Brown, V. A., McDonnell, J. J., Burns, D. A., & Kendall, C. (1999). The role of event water, a rapid shallow flow component, and catchment size in summer stormflow. *Journal of Hydrology*, *217*(3–4), 171–190. https://doi.org/10.1016/S0022-1694(98)00247-9

Brunner, P., & Simmons, C. T. (2012). HydroGeoSphere: A fully integrated, physically based hydrological model. *Ground Water*, *50*(2), 170–176. https://doi.org/10.1111/j.1745-6584.2011.00882.x

Campana, M. E., & Simpson, E. S. (1984). Groundwater residence times and recharge rates using a discrete-state compartment model and 14C data. *Journal of Hydrology*, *72*, 171–185. https://doi.org/10.1016/0022-1694(84)90190-2

Carrer, G. E., Klaus, J., & Pfister, L. (2019). Assessing the catchment storage function through a dual-storage concept. *Water Resources Research*, *55*(1), 476–494. https://doi.org/10.1029/2018WR022856

Cartwright, I., & Morgenstern, U. (2018). Using tritium and other geochemical tracers to address the "old water paradox" in headwater catchments. *Journal of Hydrology*, *563*, 13–21. https://doi.org/10.1016/j.jhydrol.2018.05.060

Chow, R., Frind, M. E., Frind, E. O., Jones, J. P., Sousa, M. R., Rudolph, D. L., et al. (2016). Delineating baseflow contribution areas for streams – A model and methods comparison. *Journal of Contaminant Hydrology*, *195*, 11–22. https://doi.org/10.1016/j.jconhyd.2016.11.001

Correa, A., Breuer, L., Crespo, P., Célleri, R., Feyen, J., Birkel, C., et al. (2019). Spatially distributed hydro-chemical data with temporally high-resolution is needed to adequately assess the hydrological functioning of headwater catchments. *Science of The Total Environment*, *651*, 1613–1626. https://doi.org/10.1016/j.scitotenv.2018.09.189

Correa, A., Windhorst, D., Tetzlaff, D., Crespo, P., Célleri, R., Feyen, J., et al. (2017). Temporal dynamics in dominant runoff sources and flow paths in the Andean Páramo. *Water Resources Research*, *53*(7), 5998–6017. https://doi.org/10.1002/2016WR020187

Cowie, R. M., Knowles, J. F., Dailey, K. R., Williams, M. W., Mills, T. J., & Molotch, N. P. (2017). Sources of streamflow along a headwater catchment elevational gradient. *Journal of Hydrology*, *549*, 163–178. https://doi.org/10.1016/j.jhydrol.2017.03.044

de Rooij, R., Graham, W., & Maxwell, R. M. (2013). A particle-tracking scheme for simulating pathlines in coupled surface-subsurface flows. *Advances in Water Resources*, *52*, 7–18. https://doi.org/10.1016/j.advwatres.2012.07.022

Dunne, T., & Black, R. D. (1970). Partial area contributions to storm runoff in a small New England watershed. *Water Resources Research*, *6*, 1296–1311. https://doi.org/10.1029/wr006i005p01296

Engdahl, N. B., & Maxwell, R. M. (2015). Quantifying changes in age distributions and the hydrologic balance of a highmountain watershed from climate induced variations in recharge. *Review*, *522*, 152–162. https://doi.org/10.1016/j.jhydrol.2014.12.032

Fenicia, F., Kavetski, D., Savenije, H. H. G., Clark, M. P., Schoups, G., Pfister, L., et al. (2014). Catchment properties, function, and conceptual model representation: Is there a correspondence? *Hydrological Processes*, *28*, 2451–2467. https://doi.org/10.1002/hyp.9726

Frei, S., Knorr, K. H., Peiffer, S., & Fleckenstein, J. H. (2012). Surface micro-topography causes hot spots of biogeochemical activity in wetland systems: A virtual modeling experiment. *Journal of Geophysical Research: Biogeosciences*, *117*, G00N12. https://doi.org/10.1029/2012JG002012

Glaser, B., Antonelli, M., Chini, M., Pfister, L., & Klaus, J. (2018). Technical note: Mapping surface-saturation dynamics with thermal infrared imagery. *Hydrology and Earth System Sciences*, *22*(11), 5987–6003. https://doi.org/10.5194/hess-22-5987-2018

Glaser, B., Antonelli, M., Hopp, L., & Klaus, J. (2020). Intra-catchment variability of surface saturation – Insights from physically based simulations in comparison with biweekly thermal infrared image observations. *Hydrology and Earth System Sciences*, *24*(3), 1393–1413. https://doi.org/10.5194/hess-24-1393-2020

Glaser, B., Klaus, J., Frei, S., Frentress, J., Pfister, L., & Hopp, L. (2016). On the value of surface saturated area dynamics mapped with thermal infrared imagery for modeling the hillslope-riparian-stream continuum. *Water Resources Research*, *52*, 8317–8342. https://doi.org/10.1002/2015WR018414

Gordon, R. P., Lautz, L. K., McKenzie, J. M., Mark, B. G., Chavez, D., & Baraer, M. (2015). Sources and pathways of stream generation in tropical proglacial valleys of the Cordillera Blanca, Peru. *Journal of Hydrology*, *522*, 628–644. https://doi.org/10.1016/j.jhydrol.2015.01.013

Gourdol, L., Clement, R., Juilleret, J., Pfister, L., & Hissler, C. (2021). Exploring the regolith with electrical resistivity tomography in large-scale surveys: Electrode spacing-related issues and possibility. *Hydrology and Earth System Sciences*, *25*, 1785–1812. https://doi.org/10.5194/hess-25-1785-2021

Grabs, T., Bishop, K., Laudon, H., Lyon, S. W., & Seibert, J. (2012). Riparian zone hydrology and soil water total organic carbon (TOC): Implications for spatial variability and upscaling of lateral riparian TOC exports. *Biogeosciences*, *9*(10), 3901–3916. https://doi.org/10.5194/bg-9-3901-2012

Gutiérrez-Jurado, K. Y., Partington, D., Batelaan, O., Cook, P., & Shanafield, M. (2019). What triggers streamflow for intermittent rivers and ephemeral streams in low-gradient catchments in mediterranean climates. *Water Resources Research*, *55*(11), 9926–9946. https://doi.org/10.1029/2019WR025041

Harms, T. K., & Grimm, N. B. (2008). Hot spots and hot moments of carbon and nitrogen dynamics in a semiarid riparian zone. *Journal of Geophysical Research*, *113*, G01020. https://doi.org/10.1029/2007JG000588

Hewlett, J. D., & Hibbert, A. R. (1967). Factors affecting the response of small watersheds to precipitation in humid areas. In W. E. Sopper, & H. W. Lull (Eds.), *International symposium on forest hydrology* (pp. 275–290). Pergamon Press. Retrieved from http://coweeta.ecology.uga.edu/publications/851.pdf

HydroAlgorithmics Pty Ltd. (2016). *AlgoMesh user guide*. Retrieved from https://static1.squarespace.com/static/569e33fad82d5e0d877c25d7/t/57b28ab6579fb3a225563e6e/1471318805055/AlgoMesh+User+Guide+v1.2.pdf

Jones, J. P., Sudicky, E. A., Brookfield, A. E., & Park, Y.-J. (2006). An assessment of the tracer-based approach to quantifying groundwater contributions to streamflow. *Water Resources Research*, *42*(2). https://doi.org/10.1029/2005wr004130

Juilleret, J., Dondeyne, S., Vancampenhout, K., Deckers, J., & Hissler, C. (2016). Mind the gap: A classification system for integrating the subsolum into soil surveys. *Geoderma*, *264*, 332–339. https://doi.org/10.1016/j.geoderma.2015.08.031

Kirchner, J. W. (2003). A double paradox in catchment hydrology and geochemistry. *Hydrological Processes*, *17*, 871–874. https://doi.org/10.1002/hyp.5108

Kirchner, J. W. (2009). Catchments as simple dynamical systems: Catchment characterization, rainfall-runoff modeling, and doing hydrology backward. *Water Resources Research*, *45*(2), 1–34. https://doi.org/10.1029/2008WR006912

Klaus, J., & McDonnell, J. J. (2013). Hydrograph separation using stable isotopes: Review and evaluation. *Journal of Hydrology*, *505*, 47–64. https://doi.org/10.1016/j.jhydrol.2013.09.006

Klaus, J., Wetzel, C. E., Martinez-Carreras, N., Ector, L., & Pfister, L. (2015). A tracer to bridge the scales: On the value of diatoms for tracing fast flow path connectivity from headwaters to meso-scale catchments. *Hydrological Processes*, *29*(25), 5275–5289. https://doi.org/10.1002/hyp.10628

Kollet, S., Sulis, M., Maxwell, R. M., Paniconi, C., Putti, M., Bertoldi, G., et al. (2017). The integrated hydrologic model intercomparison project, IH-MIP2: A second set of benchmark results to diagnose integrated hydrology and feedbacks. *Water Resources Research*, *53*, 867–890. https://doi.org/10.1002/2016WR019191

Krause, S., Lewandowski, J., Grimm, N. B., Hannah, D. M., Pinay, G., McDonald, K., et al. (2017). Ecohydrological interfaces as hot spots of ecosystem processes. *Water Resources Research*, *53*(8), 6359–6376. https://doi.org/10.1002/2016WR019516

Kristensen, K. J., & Jensen, S. E. (1975). A model for estimating actual evapotranspiration from potential evapotranspiration. *Nordic Hydrology*, *6*, 170–188. https://doi.org/10.2166/nh.1975.0012

Laudon, H., Sjöblom, V., Buffam, I., Seibert, J., & Mörth, M. (2007). The role of catchment scale and landscape characteristics for runoff generation of boreal streams. *Journal of Hydrology*, *344*(3–4), 198–209. https://doi.org/10.1016/j.jhydrol.2007.07.010

Liggett, J. E., Werner, A. D., Smerdon, B. D., Partington, D., & Simmons, C. T. (2014). Fully integrated modeling of surface-subsurface solute transport and the effect of dispersion in tracer hydrograph separation. *Water Resources Research*, *50*(10), 7750–7765. https://doi.org/10.1002/2013WR015040

Mallik, A. U., Lamb, E. G., & Rasid, H. (2001). Vegetation zonation among the microhabitats in a lacustrine environment: Analysis and application of belowground species trait patterns. *Ecological Engineering*, *18*(2), 135–146. https://doi.org/10.1016/S0925-8574(01)00069-6

Martinez-Carreras, N., Hissler, C., Gourdol, L., Klaus, J., Juilleret, J., Iffly, J. F., et al. (2016). Storage controls on the generation of double peak hydrographs in a forested headwater catchment. *Journal of Hydrology*, *543*, 255–269. https://doi.org/10.1016/j.jhydrol.2016.10.004

Martinez-Carreras, N., Wetzel, C. E., Frentress, J., Ector, L., McDonnell, J. J., Hoffmann, L., et al. (2015). Hydrological connectivity inferred from diatom transport through the riparian-stream system. *Hydrology and Earth System Sciences*, *19*, 3133–3151. https://doi.org/10.5194/hess-19-3133-2015

Maxwell, R. M., Condon, L. E., Danesh-Yazdi, M., & Bearup, L. A. (2019). Exploring source water mixing and transient residence time distributions of outflow and evapotranspiration with an integrated hydrologic model and Lagrangian particle tracking approach. *Ecohydrology*, *12*(1), e2042. https://doi.org/10.1002/eco.2042

Maxwell, R. M., Putti, M., Meyerhoff, S., Delfs, J.-O., Ferguson, I. M., Ivanov, V., et al. (2014). Surface-subsurface model intercomparison: A first set of benchmark results to diagnose integrated hydrology and feedbacks. *Water Resources Research*, *50*(2), 1531–1549. https://doi.org/10.1002/2013WR013725

McDonnell, J. J. (2003). Where does water go when it rains? Moving beyond the variable source area concept of rainfall-runoff response. *Hydrological Processes*, *17*, 1869–1875. https://doi.org/10.1002/hyp.5132

McGlynn, B. L., & McDonnell, J. J. (2003). Quantifying the relative contributions of riparian and hillslope zones to catchment runoff. *Water Resources Research*, *39*(11). https://doi.org/10.1029/2003wr002091

McGlynn, B. L., McDonnell, J. J., Seibert, J., & Kendall, C. (2004). Scale effects on headwater catchment runoff timing, flow sources, and groundwater-streamflow relations. *Water Resources Research*, *40*(7), 1–14. https://doi.org/10.1029/2003WR002494

McGlynn, B. L., & Seibert, J. (2003). Distributed assessment of contributing area and riparian buffering along stream networks. *Water Resources Research*, *39*(4), 1082. https://doi.org/10.1029/2002WR001521

Megahan, W. F., & King, P. N. (1985). Identification of critical areas on forest lands for control of nonpoint sources of pollution. *Environmental Management*, *9*, 7–17. https://doi.org/10.1007/BF01871440

Paniconi, C., & Putti, M. (2015). Physically based modeling in catchment hydrology at 50: Survey and outlook. *Water Resources Research*, *51*, 7090–7129. https://doi.org/10.1002/2015WR017780

Partington, D., Brunner, P., Frei, S., Simmons, C. T., Werner, A. D., Therrien, R., et al. (2013). Interpreting streamflow generation mechanisms from integrated surface-subsurface flow models of a riparian wetland and catchment. *Water Resources Research*, *49*, 5501–5519. https://doi.org/10.1002/wrcr.20405

Partington, D., Brunner, P., Simmons, C. T., Therrien, R., Werner, A. D., Dandy, G. C., et al. (2011). A hydraulic mixing-cell method to quantify the groundwater component of streamflow within spatially distributed fully integrated surface water-groundwater flow models. *Environmental Modelling and Software*, *26*, 886–898. https://doi.org/10.1016/j.envsoft.2011.02.007

Pfister, L., Martínez-Carreras, N., Hissler, C., Klaus, J., Carrer, G. E., Stewart, M. K., et al. (2017). Bedrock geology controls on catchment storage, mixing, and release: A comparative analysis of 16 nested catchments. *Hydrological Processes*, *31*, 1828–1845. https://doi.org/10.1002/hyp.11134

Pfister, L., McDonnell, J. J., Hissler, C., & Hoffmann, L. (2010). Ground-based thermal imagery as a simple, practical tool for mapping saturated area connectivity and dynamics. *Hydrological Processes*, *24*, 3123–3132. https://doi.org/10.1002/hyp.7840

Ramey, T. L., & Richardson, J. S. (2017). Terrestrial invertebrates in the Riparian Zone: Mechanisms underlying their unique diversity. *BioScience*, *67*(9), 808–819. https://doi.org/10.1093/biosci/bix078

Remondi, F., Kirchner, J. W., Burlando, P., & Fatichi, S. (2018). Water flux tracking with a distributed hydrological model to quantify controls on the spatiotemporal variability of transit time distributions. *Water Resources Research*, *54*(4), 3081–3099. https://doi.org/10.1002/2017WR021689

Rodriguez, N. B., & Klaus, J. (2019). Catchment travel times from composite storage selection functions representing the superposition of streamflow generation processes. *Water Resources Research*, *55*(11), 9292–9314. https://doi.org/10.1029/2019WR024973

Sayama, T., & McDonnell, J. J. (2009). A new time-space accounting scheme to predict stream water residence time and hydrograph source components at the watershed scale. *Water Resources Research*, *45*(7). https://doi.org/10.1029/2008WR007549

Scaini, A., Hissler, C., Fenicia, F., Juilleret, J., Iffly, J. F., Pfister, L., et al. (2018). Hillslope response to sprinkling and natural rainfall using velocity and celerity estimates in a slate-bedrock catchment. *Journal of Hydrology*, *558*, 366–379. https://doi.org/10.1016/j.jhydrol.2017.12.011

Schilling, O. S., Gerber, C., Partington, D. J., Purtschert, R., Brennwald, M. S., Kipfer, R., et al. (2017). Advancing physically-based flow simulations of alluvial systems through atmospheric noble gases and the novel 37Ar tracer method. *Water Resources Research*, *53*(12), 10465–10490. https://doi.org/10.1002/2017WR020754

Schwab, M. P., Klaus, J., Pfister, L., & Weiler, M. (2018). Diel fluctuations of viscosity-driven riparian inflow affect streamflow DOC concentration. *Biogeosciences*, *15*, 2177–2188. https://doi.org/10.5194/bg-15-2177-2018

Sebben, M. L., Werner, A. D., Liggett, J. E., Partington, D., & Simmons, C. T. (2013). On the testing of fully integrated surface – Subsurface hydrological models. *Hydrological Processes*, *27*, 1276–1285. https://doi.org/10.1002/hyp.9630

Singer, M. B., Harrison, L. R., Donovan, P. M., Blum, J. D., & Marvin-DiPasquale, M. (2016). Hydrologic indicators of hot spots and hot moments of mercury methylation potential along river corridors. *Science of The Total Environment*, *568*(March), 697–711. https://doi.org/10.1016/j.scitotenv.2016.03.005

Sklash, M. G., & Farvolden, R. N. (1979). The role of groundwater in storm runoff. *Journal of Hydrology*, *43*, 45–65. https://doi.org/10.1016/0022-1694(79)90164-1

Weill, S., Altissimo, M., Cassiani, G., Deiana, R., Marani, M., & Putti, M. (2013). Saturated area dynamics and streamflow generation from coupled surface-subsurface simulations and field observations. *Advances in Water Resources*, *59*, 196–208. https://doi.org/10.1016/j.advwatres.2013.06.007

Williams, D. G., & Scott, R. L. (2009). Vegetation-hydrology interactions: Dynamics of riparian plant water use. In J. C. Stromberg, & B. J. Tellman (Eds.), *Ecology and conservation of the San Pedro River* (pp. 37–56). University of Arizona Press.

Wilusz, D. C., Harman, C. J., Ball, W. P., Maxwell, R. M., & Buda, A. R. (2020). Using particle tracking to understand flow paths, age distributions, and the paradoxical origins of the inverse storage effect in an experimental catchment. *Water Resources Research*, *56*, 1–26. https://doi.org/10.1029/2019WR025140

Wrede, S., Fenicia, F., Martínez-Carreras, N., Juilleret, J., Hissler, C., Krein, A., et al. (2015). Towards more systematic perceptual model development: A case study using 3 Luxembourgish catchments. *Hydrological Processes*, *29*, 2731–2750. https://doi.org/10.1002/hyp.10393

Yang, J., Heidbüchel, I., Musolff, A., Reinstorf, F., & Fleckenstein, J. H. (2018). Exploring the dynamics of transit times and subsurface mixing in a small agricultural catchment. *Water Resources Research*, *54*(3), 2317–2335. https://doi.org/10.1002/2017WR021896

Zhang, Q., Knowles, J. F., Barnes, R. T., Cowie, R. M., Rock, N., & Williams, M. W. (2018). Surface and subsurface water contributions to streamflow from a mesoscale watershed in complex mountain terrain. *Hydrological Processes*, *32*(7), 954–967. https://doi.org/10.1002/hyp.11469